1-1-2018

Layer-By-Layer Assembly of Graphene Oxide on Thermosensitive Liposomes for Photo-Chemotherapy

Mohadeseh Hashemi
University of Tehran, Tehran, Iran

Meisam Omidi
Shahid Beheshti University

Bharadwaj Muralidharan
University of Texas at Austin

Lobat Tayebi
Marquette University, lobat.tayebi@marquette.edu

Matthew J. Herpin
University of Texas at Austin

See next page for additional authors

Accepted version. *Acta Biomaterialia*, Vol. 65 (January 2018): 376-392. DOI.

Acta Biomaterialia, Vol. 65 (2018): 376-392. DOI.

Layer-by-layer assembly of graphene oxide on thermosensitive liposomes for photo-chemotherapy

Mohadeseh Hashemi
Department of Biomedical Engineering, Faculty of New Sciences and Technologies, The University of Tehran, Tehran, Iran
Meisam Omidi
Protein Research Center, Shahid Beheshti University, GC, Velenjak, Tehran, Iran
Bharadwaj Muralidharan
Department of Biomedical Engineering, The University of Texas at Austin
Lobat Tayebi
Department of Developmental Sciences, Marquette University School of Dentistry, Milwaukee
Matthew J. Herpin
Division of Pharmaceutics, College of Pharmacy, The University of Texas at Austin
Mohammad Ali Mohagheghi
Cancer Research Center, Cancer Institute of Iran, Tehran University of Medical Sciences, Tehran, Iran

Javad Mohammadi
Department of Biomedical Engineering, Faculty of New Sciences and Technologies, The University of Tehran, Tehran, Iran
Hugh D.C. Smyth
Division of Pharmaceutics, College of Pharmacy, The University of Texas at Austin
Thomas E. Milner
Department of Biomedical Engineering, The University of Texas at Austin

Abstract

Stimuli responsive polyelectrolyte nanoparticles have been developed for chemo-photothermal destruction of breast cancer cells. This novel system, called layer by layer Lipo-graph (LBL Lipo-graph), is composed of alternate layers of graphene oxide (GO) and graphene oxide conjugated poly (l-lysine) (GO-PLL) deposited on cationic liposomes encapsulating doxorubicin. Various concentrations of GO and GO-PLL were examined and the optimal LBL Lipo-graph was found to have a particle size of 267.9 ± 13 nm, zeta potential of +43.9 ± 6.9 mV and encapsulation efficiency of 86.4 ± 4.7%. The morphology of LBL Lipo-graph was examined by cryogenic-transmission electron microscopy (Cryo-TEM), atomic force microcopy (AFM) and scanning electron microscopy (SEM). The buildup of LBL Lipo-graph was confirmed via ultraviolet-visible (UV–Vis) spectrophotometry, thermogravimetric analysis (TGA) and differential scanning calorimetry (DSC) analysis. Infra-red (IR) response suggests that four layers are sufficient to induce a gel-to-liquid phase transition in response to near infra-red (NIR) laser irradiation. Light-matter interaction of LBL Lipo-graph was studied by calculating the absorption cross section in the frequency domain by utilizing Fourier analysis. Drug release assay indicates that the LBL Lipo-graph releases much faster in an acidic environment than a liposome control. A cytotoxicity assay was conducted to prove the efficacy of LBL Lipo-graph to destroy MD-MB-231 cells in response to NIR laser emission. Also, image stream flow cytometry and two photon microcopy provide supportive data for the potential application of LBL Lipo-graph for photothermal therapy. Study results suggest the novel dual-sensitive nanoparticles allow intracellular doxorubin delivery and respond to either acidic environments or NIR excitation.

Statement of Significance

Stimuli sensitive hybrid nanoparticles have been synthesized using a layer-by-layer technique and demonstrated for dual chemo-photothermal destruction of breast cancer cells. The hybrid nanoparticles are composed of alternating layers of graphene oxide and graphene oxide conjugated poly-l-lysine coating the surface of a thermosensitive cationic liposome containing doxorubicin as a core. Data suggests that the hybrid nanoparticles may offer many advantages for chemo-photothermal therapy. Advantages include a decrease of the initial burst release which may result in the reduction in systemic toxicity, increase in pH responsivity around the tumor environment and improved NIR light absorption.

Graphical abstract

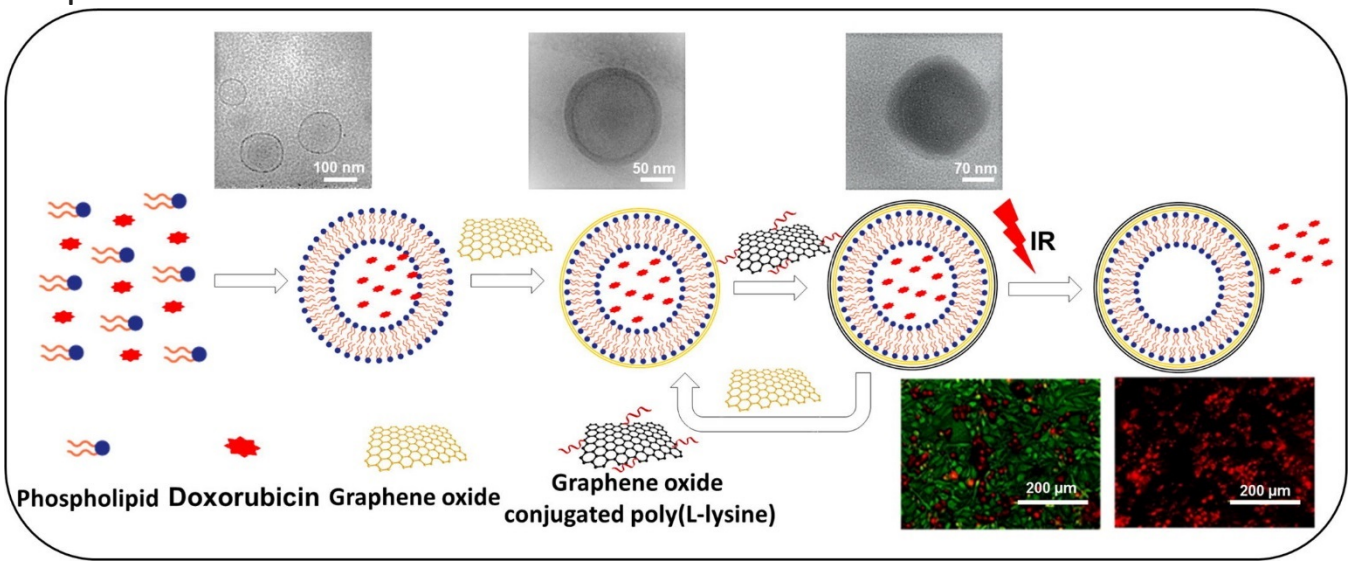

Keywords

Liposome, Graphene oxide, Thermosensitive, Layer by layer

1. Introduction

Liposomes have been one of the most investigated drug delivery systems, especially in clinically relevant cancer models.[1,2] In recent years, important advances to improve the therapeutic effect and targeting of administered drugs to cancer patients have been made.[3,4,5,6] In particular, efficacy of treatment is highly dependent on the presence of sufficient drug in the tumorigenic region.[1,7] This, in turn, is dependent on effective delivery via a high payload capacity, high cellular uptake, and also programmed drug release.[8] Recently, a layer-by-layer deposition method has been shown to be an effective process to improve therapeutic efficacy of administrated liposomes.[9,10,11]

Layer-by-layer liposomal nanoparticles fabricated by deposition of alternate layers of charged polyelectrolytes onto the liposomes is intriguing due to the high loading capacity, multi-functionality, tailored drug release and stimuli-responsiveness that can be achieved using this design.[12,13,14] Although some studies have focused on the application of LBL assemblies in drug delivery, the main emphasis of these studies is to fabricate barrier layers to control cargo release encapsulated in the core while fewer attempts have been made to fabricate an LBL engineered system to target tumor and facilitate site-specific triggered cargo release.[14,15,16]

A variety of stimuli sensitive LBL constructions have been reported to modify liposomes by using polyethylene glycol-reprivatized nanotubes,[17] nanogolds,[18] magnetic nanoparticles.[19] Among other stimuli sensitive delivery vehicles, near infrared (NIR) light triggered drug release has some advantages as light at this wavelength has its maximum penetration depth through the tissue, while the main interaction of tissue and light is scattering.[20,21,22] Thus, in recent years different types of photo-absorbers with NIR absorption have been investigated including gold nanorods,[23,24,25,26,27] gold nanoshells,[28,29] carbon nanotubes[30,31,32,33] and graphene oxide.[34,35]

Graphene oxide (GO) is a single layer of graphite with unique thermal, electrical and optical properties. Graphene oxide is able to absorb NIR light due to the delocalization of the electron states, and light absorption rapidly transformed into thermal energy.[34,36,37,38] Hence, GO with a large number of surface functional groups on the surface, low production cost and acceptable thermal conductivity, can be considered as a versatile stimuli-triggered candidate for photothermal therapy.[36,39,40,41,42,43] However, only a few studies have been reported on the application of GO for photothermal therapy. Yang et al., studied the influence of size and surface chemistry of GO coated PEG on photothermal destruction of cancer cells.[39] Cheng et al., examined chemo-photothermal properties of PEGylated GO containing doxorubicin on cancer cells.[44]

The interaction between graphene oxide and liposome was studied previously by Feng et al.[45,46] They studied the interaction between nondiamond, graphene oxide and carbon nanotube with zwitterionic liposomes. They found that the absorption of carbon based materials to the surface of liposomes neither induces drug leakage nor affect phase transition temperature.[45] In another study by the same group, they demonstrated that the absorption of DOPC and doxorubicin on the surface of graphene oxide was orthogonal because doxorubicin and DOPC didn't displace each other and the adsorption capacity was dependent on the presence of other molecules.[46]

In the current studies, we sought to improve the bioavailability and also pharmacokinetic profile of nanoparticles intended for tumorigenic delivery by combining the advantages of liposomes with a layer-by-layer synthesis technique. We chose a combination of GO and GO-PLL as the respective polycation and polyanionic alternating layers and thermosensitive cationic liposome containing doxorubicin as a core to fabricate layer by layer architecture. Positively charged poly-l-lysine (PLL) is known to improve the cellular uptake of the nanoparticles and if PLL is incorporated in the LBL nanoparticles, they have the potential to advance clinical translation of the nanotechnology.[47] NIR light is absorbed by GO and GO-PLL and converted to heat. Photothermal energy is used to activate a liquid phase transition temperature of the phospholipid membrane and lead to the release of the encapsulated toxic cargo. The present study investigates the concentration required for layer-by-layer fabrication of GO and GO-PLL on the liposomal core (LBL Lipo-graph) and their physiochemical characterization. The light matter interaction was studied by calculation the cross section absorption of LBL Lipo-graph at 808 nm pulse laser irradiation in the frequency domain by utilizing the Fourier analysis. Cytotoxicity analysis of LBL Lipo-graph were performed on MD-MB-231 cell lines. The interaction of LBL Lipo-graph with MD-MB-231 cell lines was analyzed by image stream flow cytometry and confocal microcopy.

2. Materials and method

2.1. Materials

Graphene oxide was purchased from Graphene Supermarket (Reading, MA, USA). 1,2-dipalmitoyl-sn-glycerol-3-phosphatidylcholine (DPPC), cholesterol (Chol), 1 2-Dioleoyloxy-3-trimethylammonium propane chloride (Dotap) and poly(l-lysine) (PLL, MW: 15,000–30,000) were obtained from Avanti Polar Lipids Inc. (Alabaster, AL). Polyoxyethylene (20) stearyl ether (Brij 78), doxorubicin HCl (DOX), fetal bovine serum (FBS), phosphate buffer saline (PBS), and Dulbecco's Modified Eagle Medium (DMEM) and Cell Proliferation Reagent Kit I (MTT) were purchased from Sigma Aldrich (USA). Fluorescein-5-Isothiocyanate (FITC) and Live/dead cellular viability assay kits were purchased from Thermo-Fisher. PE (Lissamine Rhodamine B) was purchased from Avanti Polar Lipids Inc. Cell tracker green and DAPI (4',6-

diamidino-2-phenylindole) were supplied from Molecular Probe Inc. Mounted media was obtained from Vector Laboratories, CA. All other chemical agents utilized were analytical grade.

2.2. Methods

2.2.1. Preparation of GO and GO-PLL suspension

An aqueous GO suspension was probe sonicated for 3 h (100 W, 5 s on and 2 s off, Misonix, USA) to achieve exfoliated GO nano-sheets. Then, GO-PLL was prepared by vigorous stirring of 8 mg of poly-l-lysine, 2 mg of GO, and 10 mg of KOH in 10 ml of distilled water at 70 °C for 24 h following by multiple centrifugation steps with water to remove excess PLL and impurities. The GO-PLL formation was confirmed using FTIR (Perkin Elmer, Waltham, MA, USA).

2.2.2. Fabrication of LBL Lipo-graph

Thermosensitive liposomal nanoparticles (Lipo) were prepared using a thin film hydration and pH gradient loading method. Briefly, 60 μmol of lipid mixture composed of DPPC, Brij 78, Dotap and Chol in a molar ratio of 66/4/20/10 were dissolved in the mixture of chloroform/methanol (3:1) in a round bottom flask. Then the organic solvent was evaporated from the lipid phase under reduced pressure at 37 °C in a rotary evaporator (Buchi Labortechnik, Switzerland) to form a thin lipid film on the inside flask wall. Then the resulting thin lipid film was hydrated using 200 mM phosphate buffer saline at 42 °C (pH = 4). Subsequently, the large multilayered vesicles in a final concentration of 20 μmol·ml−1 (i.e. 13.72 mg·ml−1) were extruded through a 100-nm polycarbonate filter using a mini-extruder (Avanti Polar Lipids, Inc., Alabaster, USA) for 21 cycles. A transmembrane pH gradient across the membrane was induced by exchanging external sulfate buffer with PBS solution using a dialysis bag (MWCO of 10 kDa, BBI, Canada), pH = 8.4. DOX (Lipid·drug−1 = 20 (molar ratio)) was loaded into liposome by incubating for 45 min at 37 °C while stirring. Subsequently free DOX was separated using dialysis bag. All procedures were completed in a dark environment.

LBL Lipo-graph were fabricated by continuously coating the Lipo with series of polyelectrolyte suspensions of GO and GO-PLL using a layer-by-layer assembly method mediated by ionic interaction. In brief, 1 ml of 1 mg/ml of liposomes (containing DOX) were first coated by several anionic GO concentrations (= 1/2, 1/4, 1/8, 1/16 (mass ratio)) under constant magnetic stirring at 2000 rpm for 20 min followed by immediate sonication for another 10 min (Sonics, USA). Particles were then subjected to centrifugation at several speeds (0, 2000, 5000, 7000, 13,000 rpm) for 15 min. The size, polydispersity index (PDI), zeta potential and the percentage of sedimentation were analyzed in sediment and supernatant portions at each speed to study LBL Lipo-graph behavior at each centrifuge speed. To measure the percentage of liposomal sedimentation, the concentration of phospholipid was determined by the Stewart assay.[48]

1 ml of single layer coated liposome (1 LBL Lipo-graph) was then coated with GO-PLL in different mass ratio ((1-LBL Lipo-graph)/(GO-PLL) = 1/2, 1/1, 2/1) under constant stirring and sonication similar the first layer. For fabricating a 3-LBL Lipo-graph, various mass ratios of GO to 2 LBL Lipo-graph ((2-LBL Lipo-graph)/(GO) = 1/2, 1/1, 2/1, 4/1) were examined. The ultimate 4-LBL Lipo-graph were fabricated by examining the different mass ratio ((3-LBL Lipo-graph)/(GO-PLL) = 4/1, 8/1, 16/1, 32/1).

Centrifugation was done as described above in each coating step. Fig. 1 shows a schematic illustration of the process for the preparation of LBL Lipo-graph.

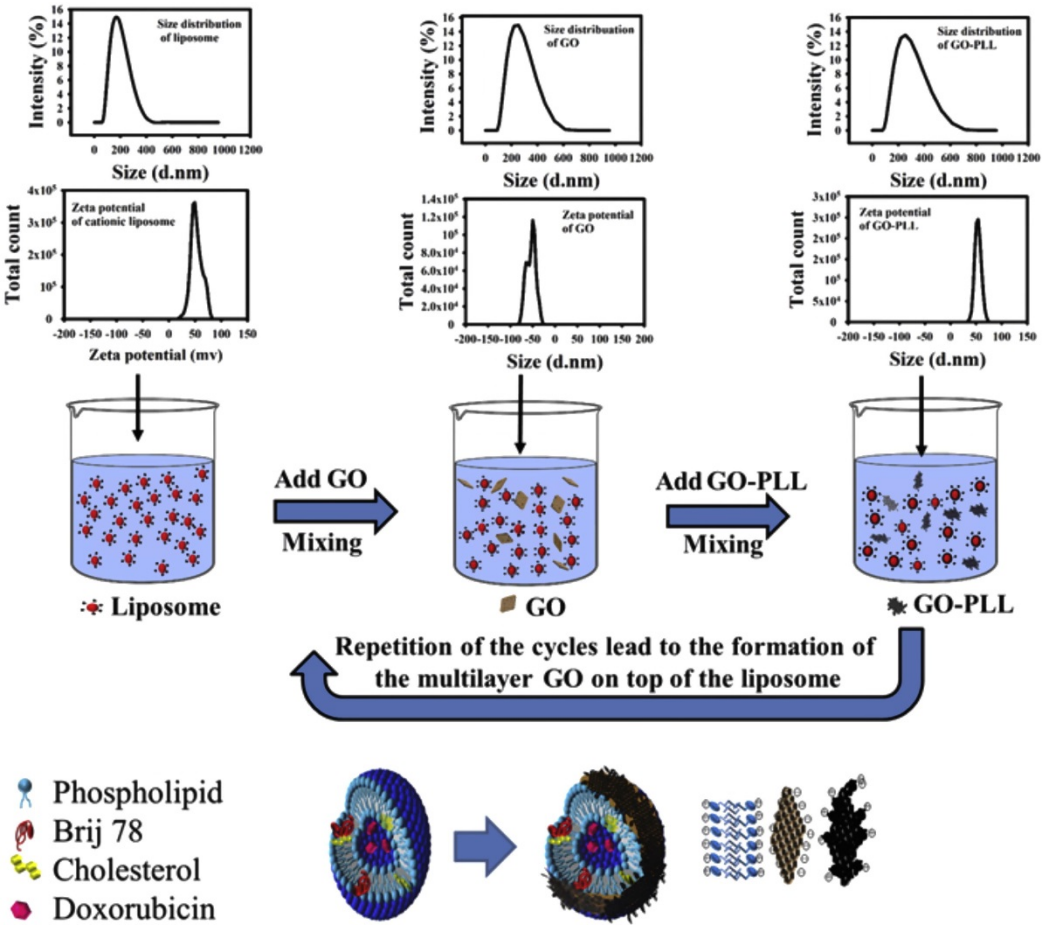

Fig. 1. Schematic representation of LBL Lipo-graph preparation by assembly of GO and GO-PLL onto a cationic thermosensitive liposome.

2.2.3. Molecular weight measurement

The molecular weight of LBL Lipo-graph was determined by Zetasizer ZS (Malvern Instruments, Malvern, UK) using static light scattering (SLS) technique as previously described by Sayari et al.[49]

Briefly, 5 different concentration of LBL Lipo-graph were prepared and the intensity of scatted light was determined. The molecular weight was measured by using the relationship between the intensity of scattered light and its size and molecular weight based on Rayleigh theory.[50] The molecular weight was determined in Da.

2.2.4. Size and zeta potential analysis of LbL Lipo-graph

The average diameter and surface charge of Lipo, LBL Lipo-graph, GO and GO-PLL were measured at 25 °C using a Zetasizer Nano ZS (Malvern Instruments, Malvern, UK). All data were calculated as the average of at least triplicate measurements.

2.2.5. Morphology characterization

The morphology was characterized by cryo-transmission electron microscopy (cryoTEM), TEM, atomic force microscopy (AFM), and scanning electron microscopy (SEM).

For Cryo-TEM study, a droplet sample was placed on a carbon coated grid (treated with plasma to increase hydrophilicity) in a controlled humidity chamber (FEI Vitrobot). The grid was then blotted by two piece of filter papers followed by plunging into liquid ethane. The grid was examined under TEM (FEI Tecnai G2 F20, FEI Company, USA) at a voltage of 200 kV. In TEM analysis, a droplet of diluted sample was placed onto a copper mesh grid and excess liquid removed with filter paper. The grids were examined under TEM (FEI Tecnai, USA) at a voltage of 80 kV. For AFM, the samples were dried on a mica substrate, and analysed by tapping mode AFM (SPM VEECO, USA).

For SEM, a droplet of samples were dried on copper grid and analysed under SEM (Hitachi S-5500 SEM/STEM, Japan) Instrument.

2.2.6. UV vis spectroscopy

LBL Lipo-graph were analyzed using UV–vis spectroscopy (Infinite M200, Tecan Systems Inc., USA).

2.2.7. Thermal analysis

Thermogravimetric analysis (TGA) was carried out using thermogravimetric analyzer (TGA Q500, TA Instruments, Delaware, US). The samples were heated from room temperature to 600 °C at a ramp rate of 10 °C/min, the data were analyzed by TA instrument software. Differential scanning calorimetry (DSC) thermograms were obtained by loading the samples into an aluminum pan and subjected to the heat cycle in a differential scanning calorimeter (DSC Q2000, TA Instruments, Delaware, US) at a ramp rate of 10°C/min from 0 to 100 °C. All the cycles were operated under a nitrogen gas atmosphere.

2.2.8. Drug loading efficiency and in vitro drug release kinetics

DOX encapsulation efficiency were determined by UV–Vis spectroscopy (Infinite M200, Tecan Systems Inc., CA, USA) at 478 nm and after complete solubilizing of Lipo by Triton X-100.

The DOX release kinetics from Liposome and LBL Lipo-graph were studied at 37, 40 and 42 °C by Mariska et al.[51] method with modification. A 200 µl of sample was diluted to 800 µl of PBS at desired temperature and were immediately incubated in 10 ml preheated PBS at 37 °C (for 24 h), 40 °C (for 30 min), and 42 °C (for 30 min) with constant stirring at 200 rpm. At each time intervals 200 µl of the medium was withdrawn and compensated by a preheated fresh medium. The DOX concentration in the samples were analyzed by UV–Vis spectroscopy at 478 nm. Also, we study the effect of pH on drug release by monitoring cumulative drug release over 24 h in PBS (pH = 7.4) and acetate-buffered saline (pH = 5.4).

2.2.9. Storage stability

Storage stability of the LBL Lipo-graph was tested at 4 °C for a week. Parameters including the zeta potential, particle size and encapsulation efficiency were evaluated.

2.2.10. LBL Lipo-graph photothermal response

LBL Lipo-graph with different layers (400 µl, 1 mg·ml−1) were transferred in 96-well plate. An 808 nm diode laser with power density of (0.5, 1 and 1.5 W·cm−2) was applied to the samples. Increasing

temperature in response to laser irradiation with a 6 mm diameter laser spot was monitored with an InSb IR camera positioned above the sample. A laser diode controller (Thorlabs, Inc., LDC 240C) regulated the diode current and a temperature controller (Thorlabs, Inc., TED 200C) fixed the emission wavelength of the laser diode. The 808 nm laser light was coupled into a multimode optical fiber (Thorlabs BFL48-1000). Light emitted from the tip of the fiber was imaged to a 6 mm diameter circular spot using an aspherical lens (f = 20 mm). The temperature was measured using a temperature calibrated InSb IR camera (FLIR systems, Inc., SC4000 MWIR).

2.2.11. Calculation of absorption cross section

The experimental setup used to measure absorption cross section of LBL Lipo-graph consists of a laser diode coupling into an optical fiber (Thorlabs BFL48-1000, USA) and emitting at 808 nm. Controllers (Thorlabs, Inc., LDC 240C and TED 200C, USA) fix current and temperature (i.e. emission wavelength) of the laser diode. Output of the multimode fiber was directed into a spherical lens (f = 20 mm) to give a 6 mm diameter spot on the surface of LBL Lipo-graph suspension. The temperature of the suspension was recorded using InSb IR camera (FLIR systems, Inc., SC4000 MWIR, USA). Acquisition control signals for IR camera frame acquisition and diode power modulation were provided by a function generator (Agilent 33250A and Berkeley Nucleonics Corp., USA) and a digital delay generator (Stanford Research Systems, Inc., DG535, USA).

To mitigate the effects of lateral thermal diffusion, a time series of radiometric images were recorded by the IR camera at various GO concentrations (0.25, 0.125, and 0.0625 mg·ml−1), GO-PLL (0.1, 0.15, and 0.2 mg·ml−1), and 4 LBL Lipo-graph (0.1, 0.2, and 0.3 mg·ml−1) placed in 96 well-plate and compared to the corresponding profile of a standard black (at 808 nm) absorber. After emission of a 25 ms pulsed laser, the first radiometric image of each samples was selected to compare the variation of the surface temperature along a diameter in the beam profile. Since the temperature profile has azimuthal symmetry, the radiometric emission profile across the beam diameter was fitted to Gaussian curve. The sample with a similar profile to the standard black paper was chosen for following calculation of absorption cross section. Calculation the cross section absorption of GO and rGO-Arg was already set up by Hashemi et al.[52]

2.2.12. In vitro photothermal response

Chemo-photothermal therapy potential of LBL Lipo-graph on MD-MB-231 cell lines were evaluated using MTT and live/dead assays. MD-MB-231 cells were seeded at a density of 50,000 cells/well in 96-well plate overnight. Then, the medium was replaced with fresh medium (composed of complete DMEM) containing different DOX concentration (0,1.25, 2.5, 5, 10 µg·ml−1) in the form of free DOX, Lipo, LBL Lipo-graph and then the plates were incubated for another 24 h. After that, cells in the laser group were exposed to NIR light (1.5 W·cm−2 with 6 mm spot size) radiation for 5 min. Then cell viability was determined by MTT assay. Briefly, 10 µl of MTT solution (5 mg·ml−1) was added to each well and incubated for 4 h. Then, 200 µl of dimethyl sulfoxide was added to each well plate and were allowed to shake for 20 min to dissolve formazan crystal.[53] The optical density of each well plate was read at 570 nm with background subtraction at 690 nm by a Tecan microplate reader (Infinite M200, Tecan Systems Inc., USA). The viability of cells was calculated by the following formula:

$$\text{mean viability} = \frac{\text{mean absorbance value of treatment group} - \text{blank}}{mean absorbance value of control - \text{blank}} \times 100$$

To visualize the effect of chemo-photothermal potential of LBL Lipo-graph, MD-MB-231 cells were stained by live/dead assay. Cell lines were seeded at a density of 50,000 cells/well in 96-well plates and incubated for 24 h prior to use. Then, cells were treated with 100 µl of LBL Lipo graph (100 µg·ml−1 of DOX) for 24 h followed by 3 times PBS washing and then exposed to NIR pulsed laser irradiation (5 min, 1 W·cm−2). After incubation for another hour, cells were stained using ethidium homodimer-1 (EthD–1) (4 M) and calcein AM (2 M) for 15 min at room temperature. Calcein AM is converted to fluorescent calcein (excitation ∼495 nm, emission ∼515 nm) by intracellular esterases present in live cells. EthD–1 penetrates the damaged cell membrane and binds to the nucleic acids (excitation ∼496 nm, emission ∼635 nm). All fluorescent images were recorded using an inverted fluorescent microscope (Evos, Life Technologies).

2.2.13. Cell association profile with LBL Lipo-graph

The percentage of cells interacting with LBL Lipo-graph and the average number of LBL Lipo-graphs per cell were analyzed by image stream flow cytometry. MD-MB-231 cell lines with density of 105 cell/well were seeded into 48-well plates for 24 h. Then, cell lines were treated with LBL Lipo-graph encapsulated FITC at a concentration of 2 × 104 LBL Lipo-graph/µl. At time intervals of 0, 1.5, 3, 6, 9 and 24 h, cells were washed with cold PBS and then were harvested by trypsinization followed by centrifugation at 4000 rpm for 5 min. The cells were resuspended in PBS and analyzed by image stream flow cytometry (Amnis Corporation, Seattle). At each time interval, at least 5000 cells were acquired and analysis was carried out only on focused cells. The fluorescent intensity arising from associated encapsulated FITC and bright filed images related to the individual cells were recorded using the extended depth of field collection mode. The data were analyzed using IDEAS software (Amnis Corporation, Seattle) to detect the number of capsules per cell.

2.2.14. LBL Lipo-graph internalization evaluation

Samples were prepared as mentioned above. Briefly, cells were treated with capsule as a ratio similar to that described above for 24 h. The cells were harvested at each time interval and resuspended in PBS for image stream flow cytometry analysis (Amnis Corporation, Seattle). Images of 5000 cells and their fluorescent intensity of FITC encapsulated in nanoparticles were recorded. The internalization analysis was performed on 200 focused single cells. IDEAS software was used to create a mask according to the bright field image and then the built-in internalization features were used to calculate the internalization score.

2.2.15. Confocal microscopy

Intracellular uptake of LBL Lipo-graph into MD-MB-231 cell lines was studied by confocal microscopy (Prairie Technologies, Inc). The cells were seeded in a 6-well plate at a density of 2 × 105 cell/well for 24 h. Then cells were incubated with LBL Lipo-graph containing rhodamine PE (1% molar ratio) for 0, 1.5, 3, 6, 9 and 24 h. Then, cells were stained with cell tracker green fluorescent probe at a concentration of 4 µM in DMSO for 15 min, followed by 3× PBS washes. Then cells were fixed in 4% paraformaldehyde in PBS for 1 h. After that, nuclei were stained for 15 min using 100 µl of 0.1 µg·m−1 of Dapi followed by 3× PBS washes. Cells were mounted in medium overnight at room temperature. Morphological features were observed under confocal microscopy (Prairie Technologies, Inc).

2.2.16. Statistical analysis

The results were evaluated statistically using one-way analysis of variance (ANOVA) followed by Tukey's pairwise test at ($P \leq 0.05$). All data were expressed as the mean ± standard deviation (SD).

3. Results and discussion

3.1. Characterization of GO and GO-PLL and uncoated liposome

Lysolipid (MSPC) containing thermosensitive liposome is one of the most studied of thermo-responsive liposomal formulations.[54,55] With this formulation, the presence of lysolipid can effectively increase the rate of drug release.[56] However, in vivo administration of this formulation exhibited desorption of lysolipids from the liposomal formulation into the biological media and also creates a defect in the bilayer which caused undesirable drug release at physiological temperature during blood circulation.[57] As a solution, a new formulation composed of Brij 78 surfactant which is substituting DSPE-PEG 2000 and MSPC functionality has been developed by Tagami et al.[54] Although, this formulation which composed of DPPC/Brij 78 (96/4) increased 40% drug release in comparison with lysolipid containing thermosensitive liposome, the absence of cholesterol decreased the stability of liposome during blood circulation and shelf life.[58,59] Herein we used Brij 78 to substitute the functionality of MSPC and DSPE-PEG 2000, cholesterol to increase the stability of the liposomes and Dotap to create a cationic liposome. As shown in a recorded DSC thermogram (Fig. 4B), our formulation can be considered as a thermosensitive liposome.

Prior to coating the liposomes with GO and GO-PLL, particle size and zeta potential of GO, GO-PLL and liposome suspension were characterized using dynamic light scattering. As shown in Fig. 1 and Table 1, the liposome size distribution was monomodal with an average z diameter of 138.8 nm and a low polydispersity index of 0.12. Zeta potential measurement showed that liposomes and GO carried a charge of 52.7 ± 11.1 mV and −53.7 ± 10.4 mV, respectively. After successful conjugation of PLL to GO (see FTIR spectrum in Fig. S1) via the primary amine group of PLL and epoxy group of GO, the zeta potential of GO-PLL inverted to +50.87 ± 9.6 mV. The initial positive charge of the liposomal surface makes it a good candidate for coating with negatively charged graphene oxide. Also, the inverse charge of GO and GO-PLL make them suitable candidates for layer-by-layer construction over the cationic thermosensitive liposome.

A)

Number of layers	GO or GO-PLL / n LBL Lipo-graph mass ratio	Z average diameter (nm)	mean PDI	zeta potential (mV)
0	0	138.8	0.12	52.7 ± 11.1
1	1/16	137.3	0.24	43.6 ± 7.8
1	1/8	134.2	0.14	25.5 ± 6.1
1	1/4	aggregate	aggregate	1.3 ± 5.2
1	1/2	153.9	0.12	-32.6 ± 4.8
1	1/1	175.3	0.16	- 38.5 ± 6.8
2	1/2	aggregate	aggregate	-9.8 ± 7.3
2	1/1	140.7	0.18	50.9 ± 8.5
2	2/1	243.8	0.10	39.9 ± 5.7
3	1/2	aggregate	aggregate	21.9 ± 8.4
3	1/1	aggregate	aggregate	-2.6 ± 6.9
3	2/1	170.7	0.17	-30.8 ± 7.9
3	4/1	258.4	0.15	-40.9 ± 3.2
4	4/1	aggregate	aggregate	-20.9 ± 7.3
4	8/1	aggregate	aggregate	8.3 ± 5.2
4	16/1	235.4	0.19	34.8 ± 5.9
4	32/1	267.9	0.173	43.9 ± 6.9

B)

GO / Liposome Mass ratio	GO / Liposome Molar ratio
0	0
1/16	0.2
1/8	0.4
1/4	0.8
1/2	1.6
1/1	3.2

Table 1. (A) Optimization of GO or GO-PLL/n LBL Lipo-graph gram ratio, (B) converting the gram ratio of GO and Liposome in single layer coated liposome to molar ratio.

Since the fabrication of LBL Lipo-graph was dependent on the electrostatic interaction of the compartments, effect of ionic strength and pH value of the working solution were examined (Fig. S2).

As shown in Fig. S2A, increasing the ionic strength decreasing the electrostatic absorption force between the GO and GO-PLL sheets which was confirmed by monitoring the zeta potential values of GO and GO-PLL at different ionic strengths. By increasing NaCl concentration, the zeta potential decreased for both GO and GO-PLL. As shown in Fig. S2A, increasing the NaCl concentration from 0 to 10 mmol·L−1 lead to a significant change in zeta potential values while further increases in NaCl concentration didn't effectively change the zeta potential. As shown in Fig. S2, to further investigate the effect of protonation and deprotonation on the electrostatic interaction, the effect of pH on zeta potential of GO, GO-PLL and cationic liposome at the same ionic concentration (10 mmol·L−1 NaCl) has been monitored. The data suggests that pH strongly impacts the surface charge density. Due to the protonation of GO sheets at lower pH and deprotonation of GO-PLL sheets at higher pH the zeta potential changed significantly at lower and higher pH for GO and GO-PLL, respectively.

Since the large difference in zeta potential values is expected to impact electrostatic interactions while using the ionic working solution increases the repeatability of the electrostatic dependent fabrication process, 10 mmol·L−1 NaCl at pH=7.4 was selected as a working solution. Our result is consistent with previously reported results.[60,61]

3.2. LbL Lipo-graph assembly: Static light scattering (SLS), dynamic light scattering (DLS) and zeta potential analysis

Sequential GO and GO-PLL nano-sheets were assembled directly on the surface of cationic liposomes to construct the LBL Lipo-graph. GO was selected as the polyanionic species due to the high negative charge density and biocompatibility. Analogously, GO-PLL was selected due to its high positive charge density, biocompatibility and cell adhesion property.[62] For fabrication of multilayered GO and GO-PLL structures, at each step, the surface must reach an opposite charge of sufficiently high magnitude to assure that the following layer is appropriately attracted to the surface. The principle of the overall approach is represented in Fig. 1 as the zeta potential and size of the uncoated liposome, GO and GO-PLL. In the present study, we showed that carful adjustment of GO and GO-PLL ratios played a significant role in the formation of LBL Lipo-graph. So, in each layer formation during LBL construction, several concentrations of GO or GO-PLL to liposome has been studied (Table 1) and the zeta potential and z average diameter of the fabricated nanoparticle has been measured.

Since the zeta potential of the liposomes were initially positive due to the presence of positively charged Dotap in the liposomal formulation we first deposited GO onto the liposome. Different GO/ Liposome mass ratios (1/16, 1/8, 1/4, 1/2, 1/1) have been examined to find an appropriate concentration of GO. As shown in Table 1, the GO/Lipo = 1/16 and 1/8 wasn't sufficient to invert the positively charge of a cationic liposome to a negative charge. While a number ratio of GO/Lipo = 1/4 caused aggregation (Supplementary 4).

At the mass ratio of GO/Lipo = 1/2 and 1/1, positively charged liposomes inverted to negatively charged in 1-LBL Lipo-graph indicating covering of the liposome surface with GO. Based on a calculation (Supplementary 3), the necessary molar ratio of GO/Lipo to completely cover a liposome is 3, so the mass ratio of GO/Lipo = 1/1 was selected as the appropriate concentration for coating the liposome. As shown in Table 1, with increasing the mass ratio of GO the zeta potential decreased while the z average diameter increased.

To deposit a second layer, GO-PLL at a different mass ratio (GO-PLL/ 1-LBL Lipo-graph = 1/2, 1/1, and 2/1) was selected. The ratio of GO-PLL/1-LBL Lipo-graph=1/2 formed aggregation in the medium. This aggregation could be related to the concentration at which the sum of all positive and negative charges at the shear plane of the fabricated structure is zero or it may be related to the presence of equal numbers of positive (Liposome and GO-PLL) and negative (GO) particles in solution.[63]

By using the same mass ratio of GO-PLL and 1-LBL Lipo-graph, the z average diameter was decreased and the colour of the suspension also turned into lighter tonalities (data not shown). It could be related to the strong electrostatic attraction between the GO-PLL and GO that apparently led to a loss of integrity between the outer layer which is a severe destabilization. The mass ratio of GO-PLL/1-LBL Lipo-graph = 2/1 has been chosen for coating in the subsequent steps.

For third and fourth layer formations several ratios of GO and GO-PLL to fabricated an LBL Lipo-graph has been examined (Table 1). Some ratios of GO or GO-PLL thus make big aggregation. The green box shows the concentration of GO or GO-PLL which cause detach of the underlying layer and blue box shows the selected concentration.

DLS analysis indicates that LBL Lipo-graph was accompanied by reaching a final size of 267.9 nm after assembly of 4 layers. The large increase in LBL Lipo-graph size after construction of 4 layers maybe related to the thick interface on the liposome surface or a disordered assembly of GO and GO-PLL. Also, SLS measurements showed that the molecular weight of Lipo-graph gradually increased by increasing the number of layers. The molecular weight of liposome, 1-LBL Lipo-graph, 2-LBL Lipo-graph, 3-LBL Lipo-graph and 4-LBL Lipo-graph was 119263 ± 10283, 452649 ± 39268, 1384842 ± 147591, and 1720382 ± 196393, 2168485 ± 246839 kDa. Large molecular weight of the fabricated LBL Lipo-graph lead to the presence of large sheets of GO and GO-PLL. The variation observed in SLS data were related to the presence of the giant molecules of LBL Lipo-graph and also presence of 2-D nanosheets of GO and Go-PLL which assumed as a spherical structure.[64]

3.3. Optimization of centrifuge speed

Centrifuge speed is considered as an important parameter during construction of LBL Lipo-graphs to separate aggregated nanoparticles from assembled LBL Lipo-graph. As shown in Fig. 2, the effect of centrifuge speed on z average diameter, polydispersity index, zeta potential and nanoparticle sedimentation were analyzed in sediment and supernatant portions of microtube after each layer formation.

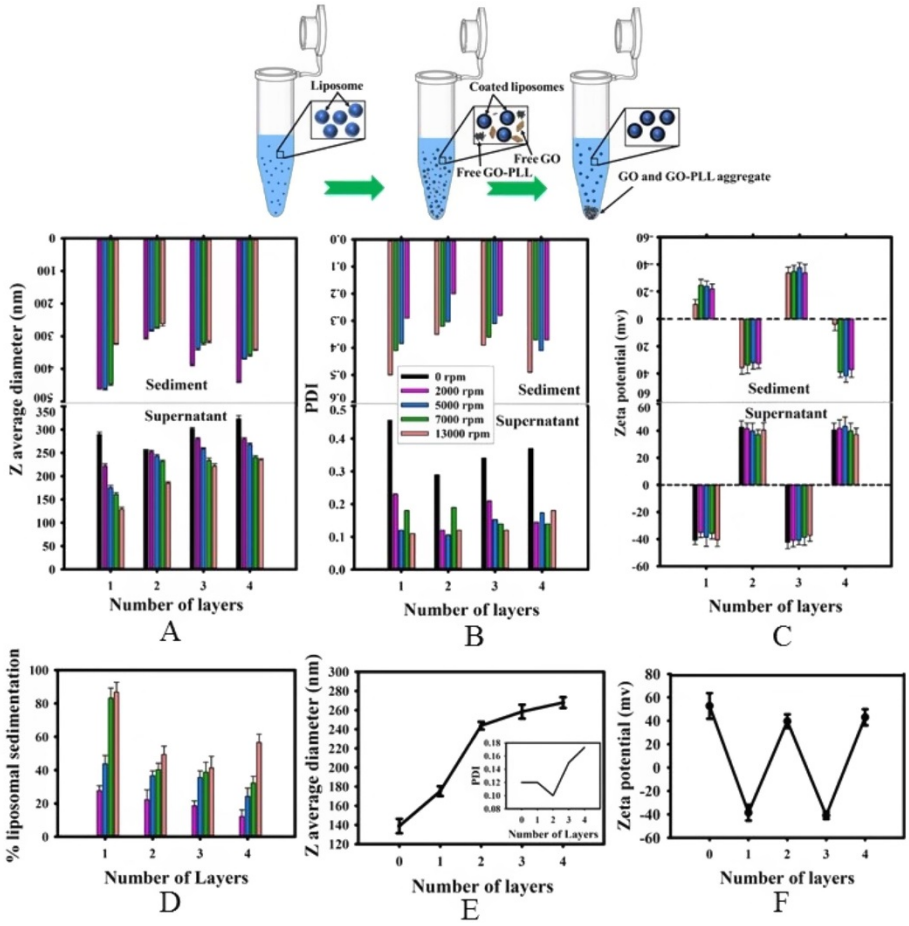

Fig. 2. The effect of centrifuge speed on (A) z average diameter, (B) PDI, and (C) Zeta potential of the nanoparticles in supernatant and sediment portion per layer formation, (D) the percentage of liposomal sedimentation per layer formation during centrifugation. Changes in (E) z average diameter, and (F) zeta potential with the addition of each polyelectrolyte layer on the cationic liposome.

In the supernatant, the size of an LBL Lipo-graph decreased with increased centrifuge speed while in the sediment portion the size of nanoparticle increased after each layer formation. Without centrifugation, size of 1-LBL Lipo-graph was 289.5 ± 5.2 nm, which is larger than the size of individual liposomes and graphene oxide and shows the electrostatic attachment of some liposomes and graphene oxide. High polydispersity index (PDI) (0.45, Fig. 2B) of 1-LBL Lipo-graph shows a large variability in particle size.

At 5000 rpm, size and PDI of 1-LBL Lipo-graph in supernatant was around 175.3 ± 4.3 nm and 0.12, respectively indicating that the centrifuge speed is sufficient to separate the aggregated nanoparticles from the assembled ones. As shown in Fig. 2A, B, and D since the centrifuge speed need to be as low as possible to prevent sedimentation of desired assembled LBL Lipo-graph, 5000 rpm was selected for subsequent coating steps.

As shown in Fig. 2C, no significant change in zeta potential was observed by increasing the centrifuge speed in the supernatant portion, while in the sediment portion after 13,000 rpm, the zeta potential was almost close to zero specially after deposition of the fourth layer. Two possible explanations are offered for this observation. One possibility is that LBL Lipo-graph was not sufficiently stable at 13000 rpm centrifugation and lead to the formation of large aggregation composed of 56.5 ± 5% liposomes (Fig. 2D).[65] A second possibility is that during high speed centrifugation, the layer-by-layer formation

structure breaks apart and GO coat charged group existing on the surface of GO-PLL and cationic liposome.[66,67]

Fig. 2D represent the results of the Stewart assay to analyze the liposomal sedimentation during centrifugation. At a 5000 rpm centrifuge speed, in the first layer formation, around 43.7% of nanoparticles were aggregated, while after coating the second layer 36.65% of nanoparticles were aggregated. After third and fourth layer formation, 35.6% and 24.2% of nanoparticles were aggregated, respectively. In other word during LBL construction almost 17.36% of liposomes were coated by GO and GO-PLL.

As discussed previously, DLS analysis indicates that LBL Lipo-graph was accompanied by a gradual increase in particle size reaching a final z average diameter of 253.4 nm and polydispersity index of 0.17 (Fig. 2E). As shown in Fig. 2F, LBL assembly was attended by a reversal of surface charge. An inversion in the LBL Lipo-graph surface charge was observed after each layer formation. However, since important functional groups such as carboxyl and amine were involved in electrostatic interaction during LBL assembly, it is likely that free functional groups were still available for further modification of the LBL Lipo-graph due to the high surface charge density of 4-LBL Lipo-graphs.[68,69]

3.4. Morphology analysis

To estimate whether liposomes were coated with GO and GO-PLL and to study the structural morphology of liposome and LBL Lipo-graph, TEM, AFM and SEM images of the samples were recorded (Fig. 3). Based on recorded AFM images, liposomes (Fig. 3A) are more uniform than LBL Lipo-graph (Fig. 3C) which is consistent with the results reported by Weilin et al.,[70] and Ye et al.[71] Although, as clearly shown in Fig. 3D image, thickness of the nanoparticles increased during layer-by-layer construction (around 130 nm based on DLS and AFM results) while the individual spherical structure were unchanged. As shown in Fig. 3(D–H) Cryo-TEM photographs are consistent with AFM images and indicate that the layer-by-layer assembly of GO and GO-PLL on the liposomes doesn't alter the spherical shape. Furthermore, cryo-TEM size measurement is consistent with DLS data. The size of 1-LBL Lipo-graph slightly increased after the deposition of the first layer but maintained a spherical non-aggregated morphology (Fig. 3E and F). Thickness of GO coated liposome is about 16 nm (Fig. 3H) which is nearly equal to the value observed by DLS (~18.5 nm). Due to liposome surface curvature, the assembled graphene oxide tilted, so the electron transmission path is more obstructed at the edge in comparison to the center where graphene oxide is flat (see Fig. 3I and J), so a dark ring was observed in the 1-LBL Lipo-graph (Fig. 3F). Fig. 3E shows a partial GO liposome coating. Further layer addition resulted in the formation of dark and large particles (Fig. 3G). Although the individual layers could not be distinguished because of the electrostatic attachment of GO and GO-PLL, formation of round dark particles show the assemblage of multilayer GO and GO-PLL on the liposome surface which blocked the transmission path (Fig. 3G). The results suggest that two-dimensional GO and GO-PLL structures can completely coat the liposomal surface.

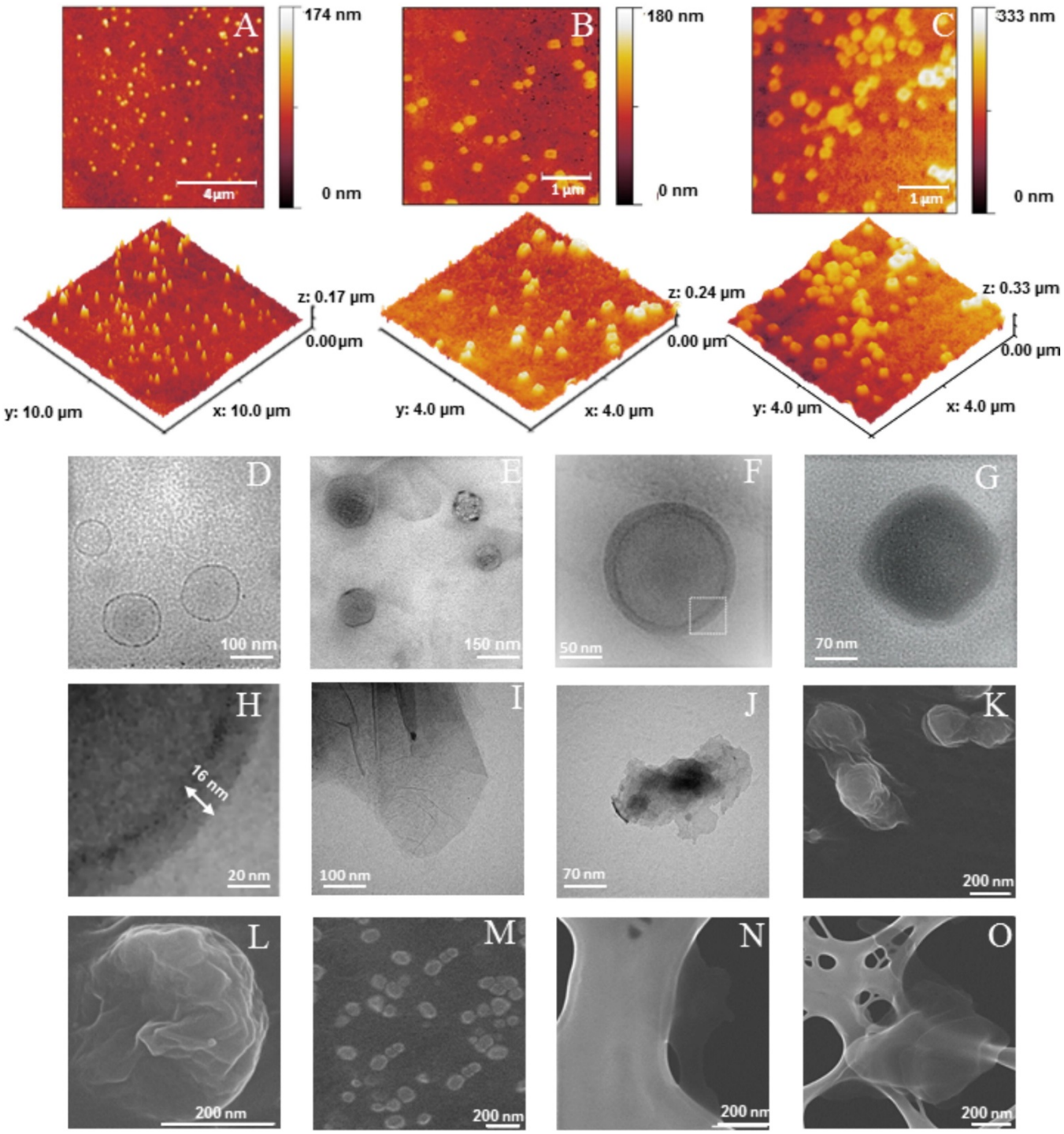

Fig. 3. AFM image of A) liposome, B) partial coated liposome, C) 4-LBL Lipo-graph. Cryo-TEM image of D) liposome, E) partial coated liposome, F) 1-LBL Lipo-graph, G) 4-LBL Lipo-graph, H) magnification of F to determine the thickness of the first layer coated liposome. TEM image of I) GO and J) GO-PLL. SEM image of K) and L) 4-LBL Lipo-graph, M) liposome, N) GO and O) multilayer GO-PLL.

Surface texture and morphology of LBL Lipo-graph nanoparticles were further confirmed by SEM imaging (Fig. 3K and L). Sucrose was used as a cryoprotectant to maintain nanoparticle morphology. As shown in Fig. 3. K, L and M liposome and LBL Lipo-graph are spherical, but as mentioned previously LBL Lipo-graphs are less uniform than liposomes. LBL Lipo-graph exhibits rarely smooth surface morphological structure leading to the non-uniform assembly of GO (Fig. 3N) and GO-PLL (Fig. 3O). Due

to nanoparticle shrinkage during drying, the difference between 2rd, 3rd, and 4rd layers of GO and GO-PLL could not be distinguished in SEM images.

3.5. Physical characterization

To investigate the photothermal potential of GO and GO-PLL, the optical absorption spectra were examined. GO displayed a strong absorption picks at ~233 and ~305 nm (Fig. S4) which are the characteristic absorption features of π-π* transition of aromatic carbon bonds and n-π* transition of carbonyl bonds,[72] respectively. After conjugation with PLL, the optical absorption increased over the entire UV–Vis spectral range representing the partial restoration of a π-network of electrically insulated GO.[60] As shown in Fig. 4A, due to the prominent absorbance for both GO and GO-PLL in the UV/Vis region the absorption strength gradually increased with each successive layer addition.

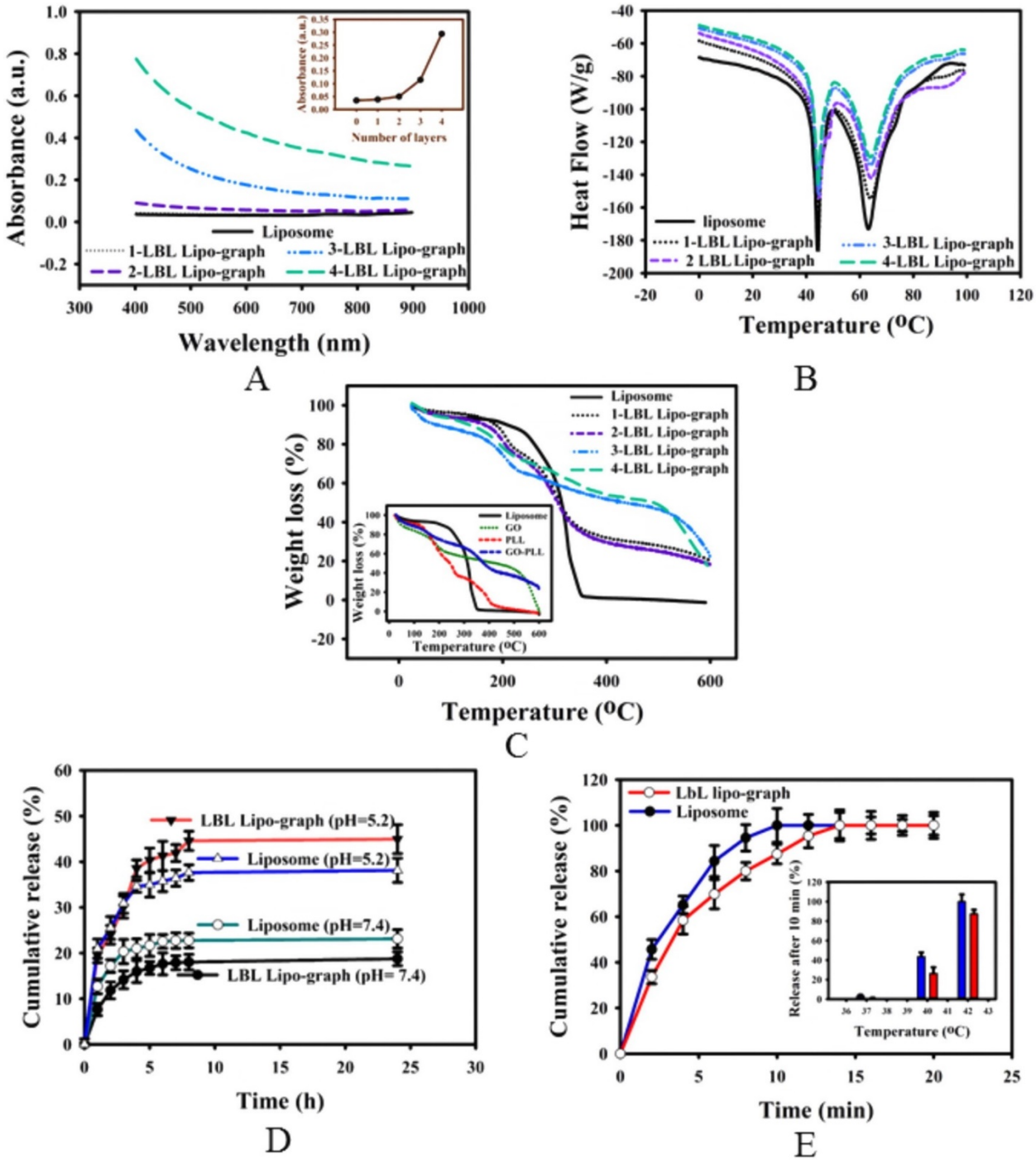

Fig. 4. (A) The absorption spectra of different particles (the inset is a plot of absorbance at 808 nm vs. the number of layers). (B) DSC and (C) TGA thermogram monitored during layer by layer construction on the thermosensitive liposome (inset is a TGA thermogram of liposome, GO, GO-PLL and PLL). Drug release assay (D) over 24 h at pH = 5.2 and pH = 7.4 and (E) during mild hyperthermia (T = 40, 42 °C) over 20 min (the inset picture is the effect of temperature on the amount of drug release over 20 min).

Furthermore, the absorption cross section of 4-LBL Lipo-graph at 808 nm as an important property to determine the ability of the photothermal transducer to absorb incident light has been calculated (see Supplementary 6).[73] To measure the absorption cross section, the effect of heat loss through the

lateral part of the sample holder was minimized by using pulse laser mode with pulse duration of 0.5 s (50% duty cycle). Then, the effect of scattering was minimized by optimizing the concentration of LBL Lipo-graph. After that, the absorption cross section was determined in the frequency domain (Fig. S5).

As shown in Table S1, the absorption cross section of 4-LBL Lipo-graph is 1.47 ± 0.1 [ml/(mg·cm)].

The results suggest that the absorption cross section of 4 LBL Lipo-graph is decreased compared to GO, due to the presence of high molecular weight phospholipid in the structure. However, the absorption cross section of 4 LBL Lipo-graph is increased as compared to bare liposome (near 0 [ml/mg·cm], data not shown).

DSC provided useful information regarding the thermotropic properties of nanoparticles following polyelectrolyte deposition by subjecting samples to a thermal cycle of heating and cooling. Thermotropic phase transitions of pure DPPC corresponds to the constant enthalpy value and melting of an acyl chain. In general, adding polymer can either increase or decrease the phase transition temperature of the main phospholipid, depending on whether it interacts with the acyl chain or polar head of phospholipid[74] and also the melting point of the main phospholipid. Our intact liposome exhibits a higher phase transition temperature (Tm = 43.29 °C) than that of pure DPPC (Tm = 39.9 °C). Although the presence of Dotap and cholesterol shift the phase transition temperature to the higher values,[75,76] Brij 78 decreased the phase temperature to lower values.[54] Importantly, the phase transition temperature slightly shifts to higher values following layer-by-layer deposition (Fig. 4B). The Tm peak broadening will increase with the number of layers and exhibit the deposition of thin layers of complementary materials on the liposome surface. A similar result was reported by Thiruganesh et al.[15] during sequential deposition of poly(ethylene glycol)-block-poly(l-aspartic acid) and poly-l-lysine on the liposomal nanoparticles. Since the melting point of pure cholesterol and Dotap is above 100 °C,[75,76] we suggest that the second peak in the DSC thermogram may be related to the total dissolution of the liposomal compartment.

Moreover, TGA was applied to evaluate the organic component in GO, GO-PLL and following assemblage of GO and GO-PLL on the liposomal nanoparticles (Fig. 4C). As shown in inset picture of Fig. 4C, in PLL the two-large shoulders on the thermal degradation curve mainly rise in around 150 and 300 °C. The plot shows a little weight loss less than 100 °C, 45% weight loss between 150 and 270 °C corresponding to the melting of PLL and a final weight loss is observed around 300 °C.[77] While for GO-PLL, up to 100 °C, the amount of weight loss is about 4% higher than GO and may lead to the incomplete drying process which attributed to the presence of heavy chain of poly(l-lysine) in the GO structure. Furthermore, in the range of 100–200 °C, GO-PLL and GO show 26% and 34% weight loss, respectively. The weight loss in the temperature range of 100-200°C is mainly related to the presence of labile oxygen in GO and GO-PLL., Conjugation of PLL to GO decreased the amount of labile oxygen in GO-PLL structures.[77,78,79] 21% of the weight loss between 300 and 400 °C in the GO-PLL may be related to the evaporation of the large portion of PLL.[77] Above 350 °C, GO exhibits 13% more weight loss than GO-PLL that lead to the carbon pyrolization.[77,78,79] Comparing the slopes of the TGA curves for GO and GO-PLL in the temperature range from 50 to 200 °C, the decomposition rate of GO-PLL is clearly much slower, suggesting the role of the electrostatic interaction between GO and GO-PLL. Comparing the TGA thermograph of GO and GO-PLL, GO-PLL has better stability especially at temperatures higher than 400°C. As shown in Fig. 4C (inset picture) in the liposomal nanoparticles, weight loss till 100 °C corresponding to the moisture and probably the presence of Brij 78 in the structure. The main weight loss between 200 and 350 °C could be due to the whole liposomal decomposition.

Fig. 4C indicates that the amount of moisture in the 1-LBL Lipo-graph is similar to the individual liposome which evaporates up to 100°C while by increasing the number of layers the moisture residue increases between layers. Weight loss in the temperature range of 100–200 °C is around 14–16% and it didn't change significantly by increasing the number of layers; the weight loss in this temperature range is probably related to the volatile oxygen corresponding to the presence of GO and PLL. The weight loss between 200 and 350 °C for 3-LBL Lipo-graph and 4-LBL Lipo-graph is around 18–19% while the weight loss for 1-LBL Lipo-graph and 2-LBL Lipo-graph is around 49–51%. Since the weight loss at this range corresponds to lipid evaporation, the stability of LBL Lipo-graph increases after adding third and fourth layers of GO and GO-PLL. The weight loss at temperatures above 350 °C for 1-LBL Lipo-graph and 2-LBL Lipo-graph are around 14–16% while for 3-LBL Lipo-graph and 4-LBL Lipo-graph are around 38–40%. This may be related to the presence of large amounts of GO on the particle.

3.6. Drug loading and release assay

DOX ($L/D = 1/20$), was loaded into the cationic liposomes using the pH gradient method between interior of the liposomes and the buffer solution, resulting in DOX protonation inside the acidic interior and reaching high encapsulation efficiency of DOX (86.4 ± 4.7%). By comparison to control blank liposomes, DOX loading was accompanied by a slight increased zeta potential and z average diameter, 52.7 ± 11.1 to 56.8 ± 10 mV and 138.8 ± 3.6 to 142.8 ± 2.8 nm, respectively. Also, by comparing DOX encapsulation efficiency before and after of LBL formation, it seems that DOX entrapment efficiency remained intact during layer-by-layer construction.

In vitro DOX release profiles from both liposome and 4-LBL Lipo-graph were evaluated in neutral (pH = 7.4) and acidic media (pH = 5.2) as shown in Fig. 4D. Liposomes displayed biphasic release kinetics with 22.48 ± 1.67% drug release at pH = 7.4 over the first 8 h followed by sustained release over the next 16 h. In contrast, LBL Lipo-graph exhibited less initial burst release at pH = 7.4 (17.85 ± 1.71%). The faster drug release from liposomal nanoparticles might be due to the high hydrophilicity of DOX and shorter path length for diffusion into the release media. In addition, the strong polyelectrolyte effectively control drug release rate at physiologic pH environments.[15] Since tumors often generate an acidic environment, release profiles from the nanoparticles at acidic pH is important. As shown in Fig. 4D, DOX release from both liposome and LBL Lipo-graph were higher in an acidic extra-vesicular environment. The acidic release effect may be related to the protonation of phosphate salt by pH shifts from 7.4 to 5.2. This results in a weak interaction between DOX and phosphate salts and lower stability of DOX inside the liposome. Similar results were observed by other investigators.[80,81,82,83] Furthermore, the present study found that DOX release rate from LBL Lipo-graph at pH = 5.2 is 7.02 ± 0.47% faster than liposomes indicating disassembly of the shells around the liposomes. Data suggests that GO has been mildly protonated (see Supplementary 1) at pH = 5.2 and this decreased the charge density for interaction with GO-PLL resulting in shell disassembly.[84]

To examine the effect of layer-by-layer assembly on thermo-responsivity of LBL Lipo-graph nanoparticles, the temperature triggering release of both LBL Lipo-graph and liposome has been examined in water (Fig. 4E). As shown in Fig. 4E, both liposomes and LBL Lipo-graph nanoparticles reached a 100% release after 12 min. LBL Lipo-graph nanoparticles demonstrate a slightly slower drug release rate with 33.53 ± 2.9% release after 2 min and 58.43 ± 6.1% after 4 min. In comparison, liposomes demonstrate a relatively faster drug release rate with 45.66 ± 3.8% in 2 min and 65.22 ± 3.8% in 4 min. A slower drug release rate may be related to the presence of a protecting shell around the liposome decreasing the drug diffusion rate to the release media. Irrespective of the surrounding shells slightly decreasing the drug release rate, it is still sufficiently high to consider as a

good candidate for laser induced thermo-responsive potential application. As supplementary data (inset picture of Fig. 4E) compares total drug release from LBL Lipo-graph nanoparticles after 20 min at 37, 40, and 42 °C with liposomes. The amount of drug release increases with increasing temperature due to the acceleration in the phase transitions of the lipid membranes. At all examined temperatures, the amount of drug release from LBL Lipo-graph nanoparticles is slightly less than liposome due to the presence of protective shells as discussed earlier.

The data suggests that LBL Lipo-graph nanoparticles offers many benefits to be considered as a good candidate for chemo-photothermal therapy application including a decrease of the initial burst release which may result in the reduction in systemic toxicity, increase in the pH responsivity around the tumor environment and better absorption at NIR regions.

3.7. Stability

The stability of LBL Lipo-graph nanoparticles was explored by monitoring DOX encapsulation efficiency, size and zeta potential over a one-week time period at 4 °C. Observations suggest that the size and zeta potential of the nanoparticles changed a little from 267.9 ± 4.6 to 272.8 ± 3.7 nm and 43.9 ± 6.9 to 38.2 ± 4.7 mV, respectively. Encapsulation efficiency didn't change after one week in part because a 4 °C storage temperature is conducive to preserve LBL Lipo-graph integrity and moreover the electrostatic shells protects DOX from release into the media.

3.8. Evaluation of LBL Lipo-graph photothermal response at 808 nm

After finding that LBL Lipo-graph has the potential to be considered as a thermo-responsive nanoparticle, we aimed to test whether thermo-sensitivity could be achieved by utilizing GO and GO-PLL to convert light into heat. So, the effect of layer-by-layer assembly of GO and GO-PLL on the liposome surface on laser induced photothermal response of the nanoparticle was investigated under NIR pulsed irradiation at different incidence fluence rates (0.5, 1, 1.5 W·cm−2) over a time period of 120 s (Fig. 5A and B). The temperature increase was dependent on the number of layers. For example, the temperature increase of 1-LBL Lipo-graph, 2-LBL Lipo-graph, 3-LBL Lipo-graph, and 4-LBL Lipo-graph nanoparticles after 2 min NIR pulse laser irradiation with a power density of 1.5 W·cm−2 was 6.9 ± 1.7, 8.57 ± 1.3, 18.55 ± 1.1, and 26.82 ± 1.7 °C, respectively. However, the temperature increase for liposome as a control sample is 0.68 ± 0.2 °C. Photothermal response of the LBL Lipo-graph samples exhibit a power density dependent temperature increase in response to NIR irradiation (Fig. 5A). Results confirm an improvement in photo-thermal response to laser light, by increasing the graphene oxide layers on the top of liposomes. Similar effects were observed with other graphene based materials.[31,40]

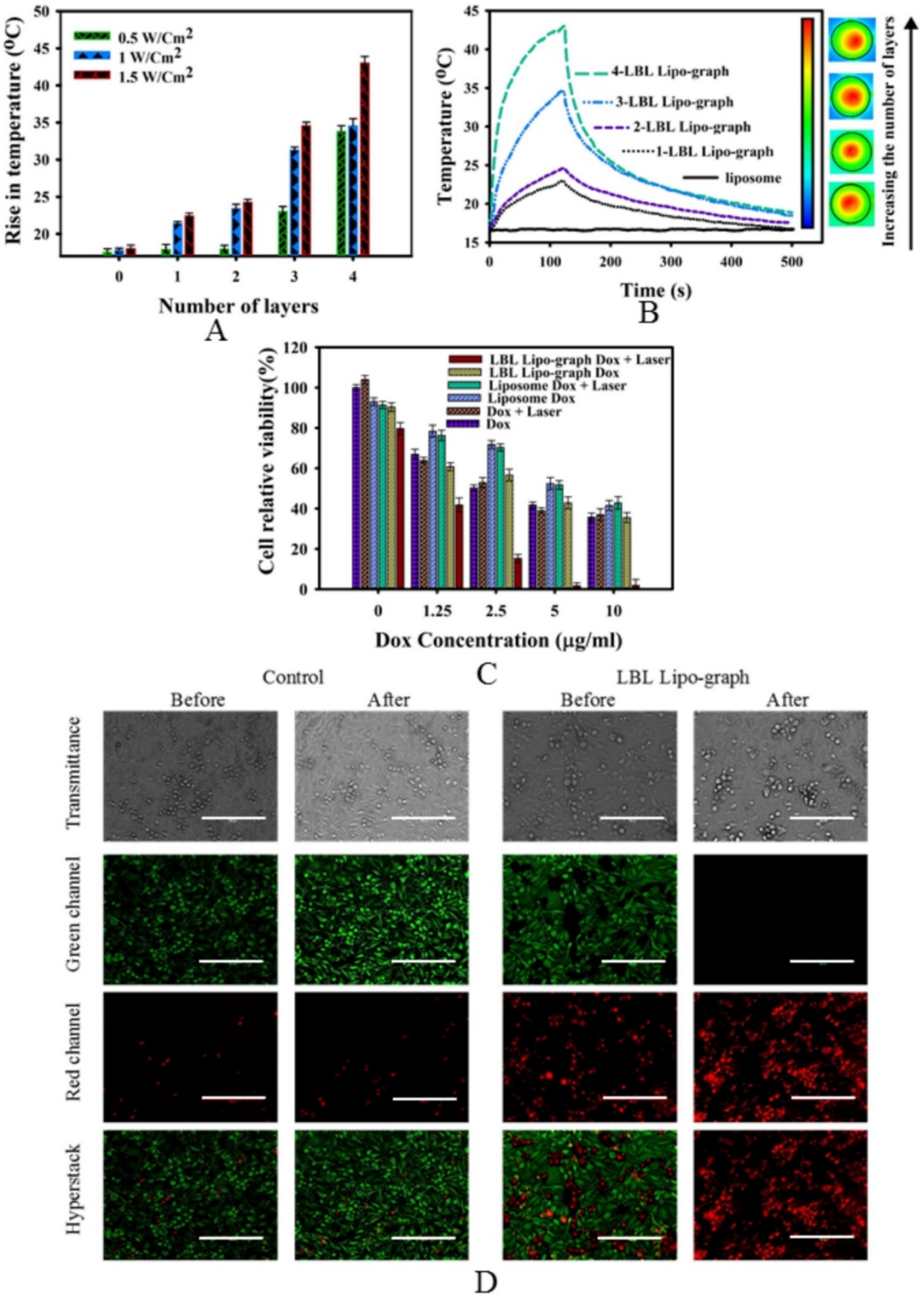

Fig. 5. Photothermal heating curve (A) at various incident NIR laser fluence (0.5, 1, 1.5 W·cm−2) and (B) during layer by layer construction (1.5 W·cm−2). (C) Cell viability of MD-MB-231 cells after incubation with LBL Lipo-graph at different DOX concentration. (D) Live/death assay of LBL Lipo-graph treated MD-MB-231 cells observed with fluorescent microscopy (The scale bar is 200 μm).

3.9. In vitro cytotoxicity assay

To further investigate whether LBL Lipo-graph encapsulated DOX can offer an effective vehicle for chemo-photothermal therapy, the antitumor effects of LBL Lipo-graph with and without NIR laser irradiation were examined on MD-MB-231 cell lines. As shown in Fig. 5C, cells were treated with several concentrations of DOX in the form of free DOX, liposome encapsulated DOX (liposome DOX), 4-LBL Lipo-graph encapsulated DOX (LBL Lipo-graph DOX) with and without NIR laser irradiation (2 min, 1.5 W·cm−2). All samples exhibited a concentration-dependent cell toxicity against MD-MB-231 (Fig. 5C).

To visualize the chemo-photothermal therapeutic potential of 4-LBL Lipo-graph on MD-MB-231 cell lines, cell lines were stained by calcein AM/ EthD–1 (Fig. 5D). Under inverted fluorescence microscope observation, dead cells exhibit red fluorescence (red channel) while live cells exhibit green fluorescence (green channels). In the group treated with 4 LBL Lipo-graph nanoparticles the cell death (red spot) before laser emission corresponded to the chemotherapy effect of DOX while after laser irradiation increased red spot represents combination of photothermal and chemotherapy targeting effect of 4-LBL Lipo-graph encapsulated DOX. As shown in Fig. 5D, no difference in toxicity levels were observed in cell groups treated without any nanoparticles before and after NIR laser irradiation.

The MTT and live/dead assay suggest that 4-LBL Lipo-graph encapsulated DOX (5 μg·ml−1) provide dual mode targeting: chemotherapy and photothermal action. NIR light absorbed by GO and GO-PLL shells is converted to heat and activates a gel to liquid phase transition of the liposomal membrane and leads to release of encapsulated DOX to destroy target tumor cells. Alternatively, light absorbed by GO and GO-PLL provide photothermal therapeutic effect to kill cancer cells.

Action of both modes are localized to minimize side effects of potential systemic cancer treatment.[24]

3.10. Cell association with LBL Lipo-graph

Motivated by the effective chemo-photothermal potential of LBL Lipo-graph nanoparticles, we studied association and number of internalized LBL Lipo-graph capsules per cell by using the image stream flow cytometry – a single platform combination of flow cytometry and fluorescent microscopy.

Images were recorded in extended depth-of-focus mode which allows a 15 μm depth into the cells and enabled quantitative analysis of the cells. The analysis was carried out by examining the individual cells which allows filtering false positive events due to the free capsule while simultaneously passing cells by the detector.

Interaction between 4-LBL Lipo-graph and cell lines are time dependent (Fig. 6A). Significant association of 4-LBL Lipo-graph with cells could be observed after several hours, with a maximum 84.9% of association after 24 h suggesting that LBL Lipo-graph binding and uptake is slow. Several studies have demonstrated that incubation time and surface chemistry have a major effect on internalization kinetics.[85,86,87,88] Although the cellular uptake of graphene oxide is slow as reported by Zhang et al.,[89] the presence of PLL on the nanomaterials surface has shown to an effective mediator on internalization via binding to anionic groups on a cell surface[90] and translocate across the membrane through an energy dependent clathrin-mediated uptake pathway.[91] Alternatively, as the incubation time increases the chance of absorbing nanoparticles onto the cell membrane for initial internalization were increased.[92,93,94] These observations are consistent with published studies that PLL-coating of nondiamond, iron oxide and rGO facilitated the cellular uptake in a time dependent manner.[95,96,97] However, specifying the exact mechanism of cellular uptake needs further investigation.

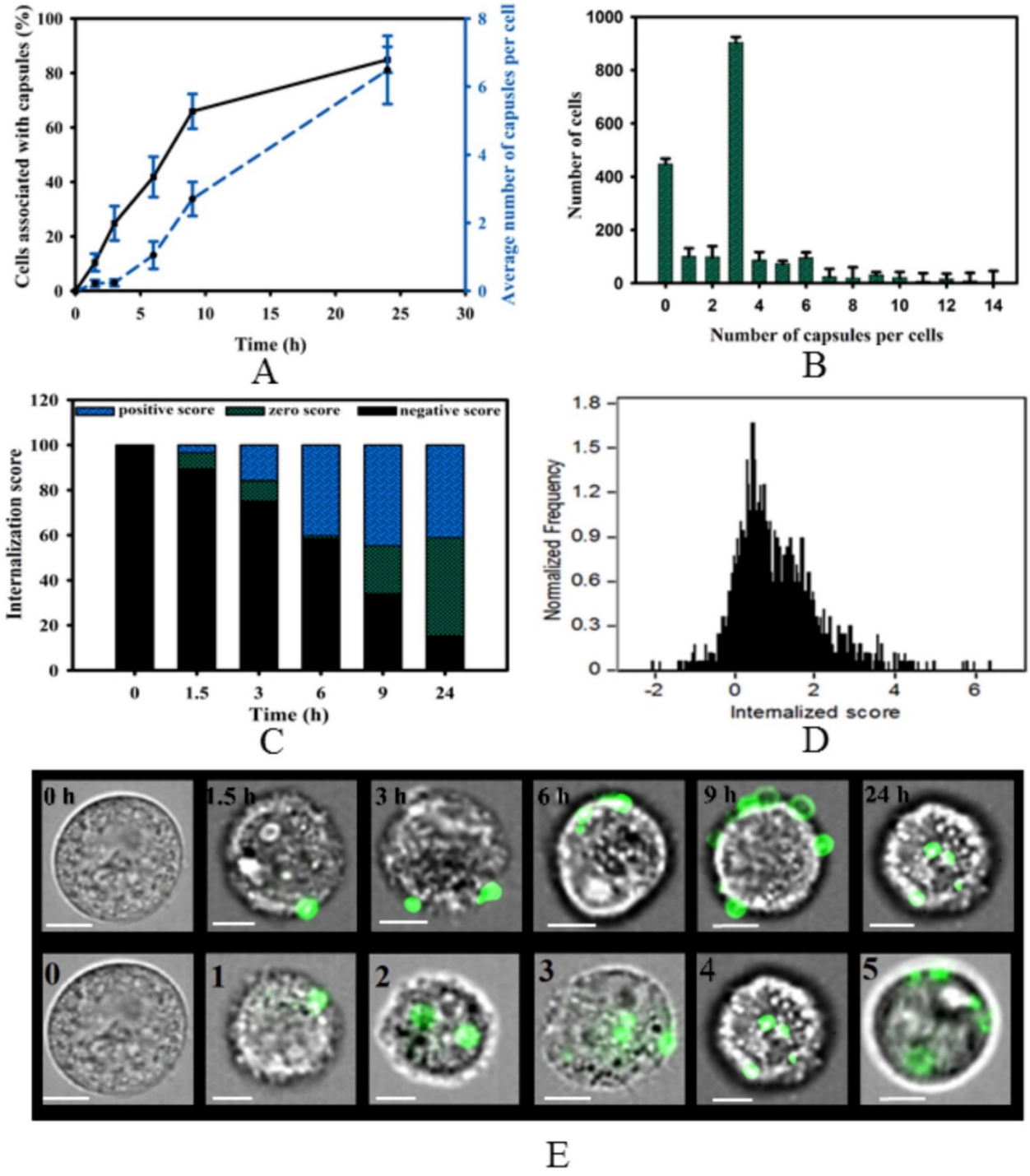

Fig. 6. Time-dependent association of FITC labelled LBL Lipo-graph with MD-MB-231 cell lines over 24 h incubation. (A) Cell percentages associated with MD-MB-231 cells after various incubation times, right y axis represents an average number of LBL Lipo-graph per cells. (B) LBL Lipo-graph distribution in cells. (C) Internalization factor monitoring during 24 h incubation. (D) Internalization factor histogram after 24 h incubation. (E) Upper row represents random cell line image after a time intervals (0, 1.5, 3, 6, 9 and 12 h) and the lower row represents examples of the cell lines with nanoparticles absorbed which are detected by an image stream flow cytometer at a particular time frame (0–5 LBL Lipo-graph/cell absorbed) (scale bar is 10 μm).

Image stream flow cytometry revealed that among all the cells associated with LBL Lipo-graph nanoparticles, an average 6 nanoparticles were endocytosed by the cells after 24 h (Fig. 6A right y-

axis). However, some cells contained larger numbers of nanoparticles (Fig. 6B). Fig. 6B shows how is the distribution of LBL Lipo-graph inside the MD-MB-231 cell lines.

The high binding and cellular uptake of LBL Lipo-graph may relate to the high positive charge of LBL Lipo-graph which leads to the presence of GO-PLL on the liposome surface. This high uptake suggested to provide a sufficient amount of therapeutic drug in the tumorigenic region.

3.11. Distinguishing the fluorescent signal from absorbed LBL Lipo-graph

Image stream flow cytometry with a normal depth of focus has been carried out to discriminate between internalized and absorbed capsules. A combination of bright field and fluorescent images of the cells enabled us to determine the internalization factor (IF) by eroding a whole cell mask and an internalized mask and then comparing them to eliminated fluorescent signals related to the non-internalized nanoparticles. A positive value of IF corresponds to an internalized nanoparticle whereas a zero value corresponds to the absorbed nanoparticles. Cells with an IF between 0 and 1 represent that nanoparticles are in the early stage of internalization. Fig. 6C monitored LBL Lipo-graph distribution in MD-MB-231 cell line after 3, 6, 9, and 24 h and Fig. 6D represented the internalization score after 24 h treated with LBL Lipo-graph. Fig. 6E upper row represents a random image of cells examined after various time intervals (0, 1.5, 3, 6, 9 and 12 h) incubation and the lower row shows the presence of 0, 1, 2, 3 and 5 nanoparticles in the cells. As shown in Fig. 6E (upper row) results suggest that after a short incubation time most nanoparticles were adsorbed on the cell surface without internalization but at longer times nanoparticles were endocytosed by the cells.

Image stream flow cytometry reveals that the nanoparticles were mainly located on the surface of the cells in shorter incubation times whereas after 24 h incubation, nanoparticles were found predominately inside the cells as well as on the cell surface. After 1.5 h, most nanoparticles have a negative internalized score indicating distribution is outside of the cells and after increasing the incubation time the negative internalized score decreased and the zero and positive internalized score increased. Results indicate movement of nanoparticles inside the cells. Understanding the main process of cellular internalization of LBL Lipo-graph will be helpful to further optimize the drug carriers for effective drug delivery.

3.12. Confocal microscopy imaging

Further characterization of LBL Lipo-graph distribution inside the cells was obtained by confocal laser scanning microscopy (Fig. 7). MD-MB-231 cells were incubated with rhodamine encapsulated LBL Lipo-graph at various incubation times. Confocal microscopy showed time dependent and highly efficient intracellular delivery of LBL Lipo-graph nanoparticles. As shown in Fig. 7A, after 24 h incubation, MD-MB-231 cells shows red dot fluorescence in the cytoplasm and nuclei, suggesting that LBL Lipo-graph were taken up by both cytoplasm and nuclei. The data was consistent with image stream flow cytometry analysis. Results indicate the presence of highly positive charged GO-PLL in the outer layers of LBL Lipo-graph increase cellular internalization over a time.

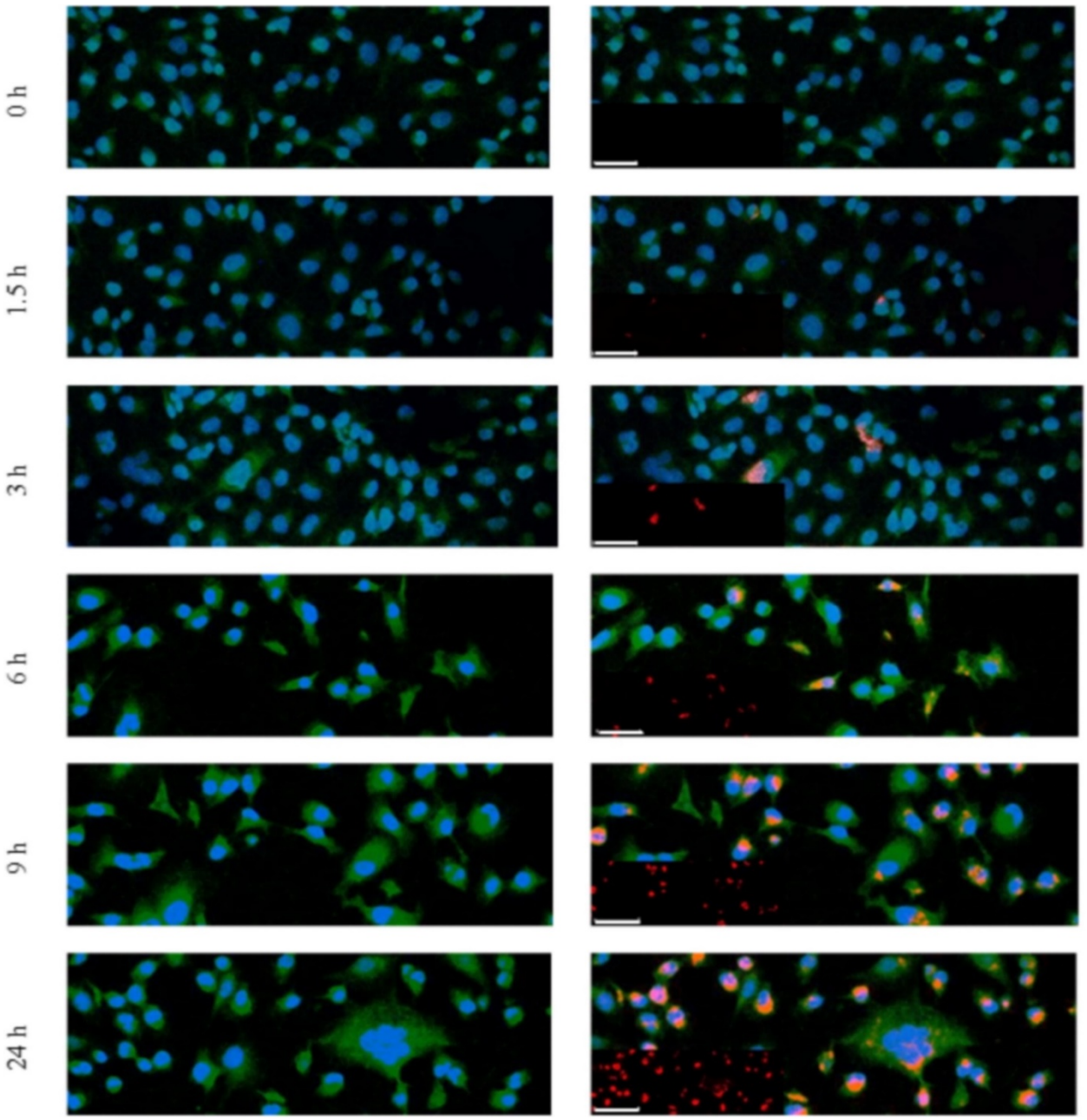

Fig. 7. The intracellular uptake of LBL Lipo-graph by MD-MB-231 cell lines was observed by confocal microscopy after 0, 1.5, 3, 6, 9 and 24 h incubation. The images obtained in the left column shows the cells and the right column represent the cells with LBL Lipo-graph internalization. The inset in the right column shows a zoomed-out version of the nanoparticles in the corresponding images. It is to be noted that colour changes occur during hyper-stacking of the images from different channels of the two photon microscope, Blue: nuclei, Green: cytoplasm, Red: LBL Lipo-graph, (scale bar is 100 μm). (For interpretation of the references to colour in this figure legend, the reader is referred to the web version of this article.)

4. Conclusion

LBL Lipo-graph encapsulated doxorubicin, a dual chemo-photothermal therapeutic platform, was successfully prepared by layer-by-layer deposition of GO and GO-PLL on the surface of cationic liposomes. The GO and GO-PLL on the liposome function as a photothermal transducer (a light

absorber and heat generating agent). The deposition of these layers was governed by electrostatic attraction. The successful layer-by-layer construction was dependent on GO and GO-PLL concentrations. As the number of layers increase the coating becomes more difficult to construct, requiring more precise adjustment of GO and GO-PLL concentrations. The fabrication of LBL Lipo-graph was monitored using DLS and zeta potential analysis. The thermal behaviour and morphology of the nanoparticles were analysed by TGA, DSC, TEM and SEM. Furthermore, IR camera imaging was performed to determine how many layers are accurately needed to achieve a desired photothermal response. Also, light matter interaction of LBL Lipo-graph with 808 nm laser was examined by measuring absorption cross section. The drug release assay of LBL Lipo-graph demonstrated the thermosensitivity and pH sensitivity of the nanoparticles. The toxicity assay showed that LBL Lipo-graph can effectively destroy MD-MB-231 cells upon NIR irradiation. The presence of GO-PLL in the outer layer of LBL Lipo-graph can increase the cellular uptake and can also increase chance of drug accumulation inside the cells. Moreover, the presence of a large number of functional groups on the GO-PLL provides an effective binding platform for active targeting of LBL Lipo-graph. We anticipate that the present system could be designed for co-delivery of multiple therapeutic agent for effective dual chemo-photothermal treatment.

Acknowledgements

The work supported by the Cancer Prevention Research Institute of Texas (CPRIT) grant DP150102.

The authors would like to acknowledge the following individuals at University of Texas at Austin: Professor Brian Korgel, Professor Martin Poenie, Dr. Jeffrey Kuhn, Dr. Ashkan Yazdi, Jonathan T Peters and Dorothy Silbaugh.

Appendix A. Supplementary data

Download Word document (6MB)

Supplementary data 1.

References

[1]A. Sharma, U.S. Sharma. Liposomes in drug delivery: progress and limitations. *Int. J. Pharm*., 154 (2) (1997), pp. 123-140.

[2]B.M. Teo, L. Hosta-Rigau, M.E. Lynge, B. Städler. Liposome-containing polymer films and colloidal assemblies towards biomedical applications. *Nanoscale*, 6 (12) (2014), pp. 6426-6433.

[3]G.D. Leonard, T. Fojo, S.E. Bates. The role of ABC transporters in clinical practice. *Oncologist*, 8 (5) (2003), pp. 411-424.

[4]L. Luo, Y. Bian, Y. Liu, X. Zhang, M. Wang, S. Xing, L. Li, D. Gao. Combined near infrared photothermal therapy and chemotherapy using gold nanoshells coated liposomes to enhance antitumor effect. *Small*, 12 (30) (2016), pp. 4103-4112

[5]Z. Li, E. Ye, R. Lakshminarayanan, X.J. Loh. Recent advances of using hybrid nanocarriers in remotely controlled therapeutic delivery. *Small*, 12 (35) (2016), pp. 4782-4806.

[6]K.Y. Choi, G. Liu, S. Lee, X. Chen. Theranostic nanoplatforms for simultaneous cancer imaging and therapy: current approaches and future perspectives. *Nanoscale*, 4 (2) (2012), pp. 330-342.

[7]C.-J. Chiou, L.-P. Tseng, M.-C. Deng, P.-R. Jiang, S.-L. Tasi, T.-W. Chung, Y.-Y. Huang, D.-Z. Liu. Mucoadhesive liposomes for intranasal immunization with an avian influenza virus vaccine in chickens. *Biomaterials*, 30 (29) (2009), pp. 5862-5868.

[8]K.S. Oh, H. Lee, J.Y. Kim, E.J. Koo, E.H. Lee, J.H. Park, S.Y. Kim, K. Kim, I.C. Kwon, S.H. Yuk. The multilayer nanoparticles formed by layer by layer approach for cancer-targeting therapy. *J. Controll. Release*, 165 (1) (2013), pp. 9-15.

[9]K. Ariga, Y.M. Lvov, K. Kawakami, Q. Ji, J.P. Hill. Layer-by-layer self-assembled shells for drug delivery. *Adv. Drug Deliv. Rev*., 63 (9) (2011), pp. 762-771.

[10]Z.J. Deng, S.W. Morton, E. Ben-Akiva, E.C. Dreaden, K.E. Shopsowitz, P.T. Hammond. Layer-by-layer nanoparticles for systemic codelivery of an anticancer drug and siRNA for potential triple-negative breast cancer treatment. *ACS Nano*, 7 (11) (2013), pp. 9571-9584.

[11]X. Liu, A. Situ, Y. Kang, K.R. Villabroza, Y. Liao, C.H. Chang, T. Donahue, A.E. Nel, H. Meng. Irinotecan delivery by lipid-coated mesoporous silica nanoparticles shows improved efficacy and safety over liposomes for pancreatic cancer. *ACS Nano*, 10 (2) (2016), pp. 2702-2715.

[12]L.J. De Cock, S. De Koker, B.G. De Geest, J. Grooten, C. Vervaet, J.P. Remon, G.B. Sukhorukov, M.N. Antipina. Polymeric multilayer capsules in drug delivery. *Angew. Chem. Int. Ed*., 49 (39) (2010), pp. 6954-6973.

[13]L.L. del Mercato, P. Rivera-Gil, A.Z. Abbasi, M. Ochs, C. Ganas, I. Zins, C. Sönnichsen, W.J. Parak. LbL multilayer capsules: recent progress and future outlook for their use in life sciences. *Nanoscale*, 2 (4) (2010), pp. 458-467.

[14]S. Simovic, T.J. Barnes, A. Tan, C.A. Prestidge. Assembling nanoparticle coatings to improve the drug delivery performance of lipid based colloids. *Nanoscale*, 4 (4) (2012), pp. 1220-1230.

[15]T. Ramasamy, Z.S. Haidar, T.H. Tran, J.Y. Choi, J.-H. Jeong, B.S. Shin, H.-G. Choi, C.S. Yong, J.O. Kim. Layer-by-layer assembly of liposomal nanoparticles with PEGylated polyelectrolytes enhances systemic delivery of multiple anticancer drugs. *Acta Biomater*., 10 (12) (2014), pp. 5116-5127.

[16]A.L. Becker, A.P. Johnston, F. Caruso. Layer-by-layer-assembled capsules and films for therapeutic delivery. *Small*, 6 (17) (2010), pp. 13-35.

[17]G. Angelini, S. Boncompagni, P. De Maria, M. De Nardi, A. Fontana, C. Gasbarri, E. Menna. Layer-by-layer deposition of shortened nanotubes or polyethylene glycol-derivatized nanotubes on liposomes: a tool for increasing liposome stability. *Carbon*, 45 (13) (2007), pp. 2479-2485.

[18].S. Angelatos, B. Radt, F. Caruso. Light-responsive polyelectrolyte/gold nanoparticle microcapsules. *J. Phys. Chem.* B, 109 (7) (2005), pp. 3071-3076.

[19]J.F. Pereira da Silva Gomes, A. Rank, A. Kronenberger, J.R. Fritz, M. Winterhalter, Y. Ramaye. Polyelectrolyte-coated unilamellar nanometer-sized magnetic liposomes. *Langmuir*, 25 (12) (2009), pp. 6793-6799.

[20]P. Huang, J. Lin, W. Li, P. Rong, Z. Wang, S. Wang, X. Wang, X. Sun, M. Aronova, G. Niu. Biodegradable gold nanovesicles with an ultrastrong plasmonic coupling effect for photoacoustic imaging and photothermal therapy. *Angew. Chem*., 125 (52) (2013), pp. 14208-14214.

[21]Y. Tang, A.J. McGoron. Combined effects of laser-ICG photothermotherapy and doxorubicin chemotherapy on ovarian cancer cells. *J. Photochem. Photobiol*. B, 97 (3) (2009), pp. 138-144.

[22]F. Zhao, J. Zhou, X. Su, Y. Wang, X. Yan, S. Jia, B. Du. A smart responsive dual aptamers-targeted bubble-generating nanosystem for cancer triplex therapy and ultrasound imaging. *Small*, 13 (20) (2017).

[23]E.B. Dickerson, E.C. Dreaden, X. Huang, I.H. El-Sayed, H. Chu, S. Pushpanketh, J.F. McDonald, M.A. El-Sayed. Gold nanorod assisted near-infrared plasmonic photothermal therapy (PPTT) of squamous cell carcinoma in mice. *Cancer Lett*., 269 (1) (2008), pp. 57-66.

[24]L. Tong, Q. Wei, A. Wei, J.X. Cheng. Gold nanorods as contrast agents for biological imaging: optical properties, surface conjugation and photothermal effects. *Photochem. Photobiol*., 85 (1) (2009), pp. 21-32.

[25]S.C. Nguyen, Q. Zhang, K. Manthiram, X. Ye, J.P. Lomont, C.B. Harris, H. Weller, A.P. Alivisatos. Study of heat transfer dynamics from gold nanorods to the environment via time-resolved infrared spectroscopy. *ACS Nano*, 10 (2) (2016), pp. 2144-2151.

[26]B.-K. Jung, Y.K. Lee, J. Hong, H. Ghandehari, C.-O. Yun. Mild hyperthermia induced by gold nanorod-mediated plasmonic photothermal therapy enhances transduction and replication of oncolytic adenoviral gene delivery. *ACS Nano*, 10 (11) (2016), pp. 10533-10543.

[27]M.B. Charati, I. Lee, K.C. Hribar, J.A. Burdick. Light-sensitive polypeptide hydrogel and nanorod composites. *Small*, 6 (15) (2010), pp. 1608-1611.

[28]L.R. Hirsch, R.J. Stafford, J. Bankson, S.R. Sershen, B. Rivera, R. Price, J.D. Hazle, N.J. Halas, J.L. West. Nanoshell-mediated near-infrared thermal therapy of tumors under magnetic resonance guidance. *Proc. Natl. Acad. Sci.,* 100 (23) (2003), pp. 13549-13554.

[29]J. Yang, J. Lee, J. Kang, S.J. Oh, H.J. Ko, J.H. Son, K. Lee, J.S. Suh, Y.M. Huh, S. Haam. Smart drug-loaded polymer gold nanoshells for systemic and localized therapy of human epithelial cancer. *Adv. Mater*., 21 (43) (2009), pp. 4339-4342.

[30]X. Liu, I. Marangon, G. Melinte, C. Wilhelm, C.C. Ménard-Moyon, B.P. Pichon, O. Ersen, K. Aubertin, W. Baaziz, C. Pham-Huu. Design of covalently functionalized carbon nanotubes filled with metal oxide nanoparticles for imaging, therapy, and magnetic manipulation. *ACS Nano*, 8 (11) (2014), pp. 11290-11304.

[31]N.W.S. Kam, M. O'Connell, J.A. Wisdom, H. Dai. Carbon nanotubes as multifunctional biological transporters and near-infrared agents for selective cancer cell destruction. *Proc. Natl. Acad. Sci. U.S.A*., 102 (33) (2005), pp. 11600-11605.

[32]M.S. Khan, H.N. Abdelhamid, H.-F. Wu. Near infrared (NIR) laser mediated surface activation of graphene oxide nanoflakes for efficient antibacterial, antifungal and wound healing treatment. *Colloids Surf*. B, 127 (2015), pp. 281-291.

[33]A. Eatemadi, H. Daraee, H. Karimkhanloo, M. Kouhi, N. Zarghami, A. Akbarzadeh, M. Abasi, Y. Hanifehpour, S.W. Joo. Carbon nanotubes: properties, synthesis, purification, and medical applications. *Nanoscale Res. Lett*., 9 (1) (2014)

[34]O.C. Compton, S.T. Nguyen. Graphene oxide, highly reduced graphene oxide, and graphene: versatile building blocks for carbon-based materials. *Small*, 6 (6) (2010), pp. 711-723.

[35]J. Kim, L.J. Cote, F. Kim, W. Yuan, K.R. Shull, J. Huang. Graphene oxide sheets at interfaces. *J. Am. Chem. Soc*., 132 (23) (2010), pp. 8180-8186.
[36]M. Omidi, A. Fathinia, M. Farahani, Z. Niknam, A. Yadegari, M. Hashemi, H. Jazayeri, H. Zali, M. Zahedinik, L. Tayebi. Bio-applications of graphene composites: from bench to clinic. *Adv. 2D Mater.* (2016), pp. 433-471.
[37]F. Gunes, H.-J. Shin, C. Biswas, G.H. Han, E.S. Kim, S.J. Chae, J.-Y. Choi, Y.H. Lee. Layer-by-layer doping of few-layer graphene film. *ACS Nano*, 4 (8) (2010), pp. 4595-4600.
[38]L. Zhang, J. Xia, Q. Zhao, L. Liu, Z. Zhang. Functional graphene oxide as a nanocarrier for controlled loading and targeted delivery of mixed anticancer drugs. *Small*, 6 (4) (2010), pp. 537-544.
[39]K. Yang, S. Zhang, G. Zhang, X. Sun, S.-T. Lee, Z. Liu. Graphene in mice: ultrahigh in vivo tumor uptake and efficient photothermal therapy. *Nano Lett*., 10 (9) (2010), pp. 3318-3323.
[40]J.T. Robinson, S.M. Tabakman, Y. Liang, H. Wang, H. Sanchez Casalongue, D. Vinh, H. Dai. Ultrasmall reduced graphene oxide with high near-infrared absorbance for photothermal therapy. *J. Am. Chem. Soc*., 133 (17) (2011), pp. 6825-6831.
[41]H. Bao, Y. Pan, Y. Ping, N.G. Sahoo, T. Wu, L. Li, J. Li, L.H. Gan. Chitosan-functionalized graphene oxide as a nanocarrier for drug and gene delivery. *Small*, 7 (11) (2011), pp. 1569-1578.
[42]M. Hashemi, A. Yadegari, G. Yazdanpanah, S. Jabbehdari, M. Omidi, L. Tayebi. Functionalized R9-reduced graphene oxide as an efficient nano-carrier for hydrophobic drug delivery. *RSC Adv*., 6 (78) (2016), pp. 74072-74084.
[43]M. Hashemi, A. Yadegari, G. Yazdanpanah, M. Omidi, S. Jabbehdari, F. Haghiralsadat, F. Yazdian, L. Tayebi. Normalization of doxorubicin release from graphene oxide: New approach for optimization of effective parameters on drug loading. *Biotechnol. Appl. Biochem*., 64 (3) (2017), pp. 443-452.
[44]W. Zhang, Z. Guo, D. Huang, Z. Liu, X. Guo, H. Zhong. Synergistic effect of chemo-photothermal therapy using PEGylated graphene oxide. *Biomaterials*, 32 (33) (2011), pp. 8555-8561.
[45]F. Wang, J. Liu. Nanodiamond decorated liposomes as highly biocompatible delivery vehicles and a comparison with carbon nanotubes and graphene oxide. *Nanoscale*, 5 (24) (2013), pp. 12375-12382.
[46]F. Wang, B. Liu, A.C.F. Ip, J. Liu. Orthogonal adsorption onto nano-graphene oxide using different intermolecular forces for multiplexed delivery. *Adv. Mater*., 25 (30) (2013), pp. 4087-4092.
[47]C.H.J. Choi, C.A. Alabi, P. Webster, M.E. Davis. Mechanism of active targeting in solid tumors with transferrin-containing gold nanoparticles. *Proc. Natl. Acad. Sci*., 107 (3) (2010), pp. 1235-1240.
[48]J.C.M. Stewart. Colorimetric determination of phospholipids with ammonium ferrothiocyanate. *Anal. Biochem*., 104 (1) (1980), pp. 10-14.
[49]E. Sayari, M. Dinarvand, M. Amini, M. Azhdarzadeh, E. Mollarazi, Z. Ghasemi, F. Atyabi. MUC1 aptamer conjugated to chitosan nanoparticles, an efficient targeted carrier designed for anticancer SN38 delivery. *Int. J. Pharm*., 473 (1) (2014), pp. 304-315.
[50]R.A. Muzzarelli, C. Lough, M. Emanuelli. The molecular weight of chitosans studied by laser light-scattering. *Carbohydr. Res*., 164 (1987), pp. 433-442.
[51]M. De Smet, S. Langereis, S. van den Bosch, H. Grüll. Temperature-sensitive liposomes for doxorubicin delivery under MRI guidance. *J. Control. Release*, 143 (1) (2010), pp. 120-127.
[52]M. Hashemi, M. Omidi, B. Muralidharan, H.D. Smyth, M.A. Mohagheghi, J. Mohammadi, T.E. Milner. Evaluation of the photothermal properties of a reduced graphene oxide/arginine nanostructure for near-infrared absorption. *ACS Appl. Mater. Interfaces*, 9 (38) (2017), pp. 32607-32620.
[53]L. Xiong, B. Shen, D. Behera, S.S. Gambhir, F.T. Chin, J. Rao. Synthesis of ligand-functionalized water-soluble [18 F] YF 3 nanoparticles for PET imaging. *Nanoscale*, 5 (8) (2013), pp. 3253-3256.

[54]T. Tagami, M.J. Ernsting, S.-D. Li. Optimization of a novel and improved thermosensitive liposome formulated with DPPC and a Brij surfactant using a robust in vitro system. *J. Control. Release*, 154 (3). (2011), pp. 290-297

[55]D. Needham, J.-Y. Park, A.M. Wright, J. Tong. Materials characterization of the low temperature sensitive liposome (LTSL): effects of the lipid composition (lysolipid and DSPE–PEG2000) on the thermal transition and release of doxorubicin. *Faraday Discuss*., 161 (2013), pp. 515-534.

[56]J.K. Mills, D. Needham. Lysolipid incorporation in dipalmitoylphosphatidylcholine bilayer membranes enhances the ion permeability and drug release rates at the membrane phase transition. *Biochim. Biophys. Acta*, 1716 (2) (2005), pp. 77-96.

[57]G.N. Chiu, S.A. Abraham, L.M. Ickenstein, R. Ng, G. Karlsson, K. Edwards, E.K. Wasan, M.B. Bally. Encapsulation of doxorubicin into thermosensitive liposomes via complexation with the transition metal manganese*. J. Control. Release*, 104 (2) (2005), pp. 271-288.

[58]G. Gregoriadis, C. Davis. Stability of liposomes invivo and invitro is promoted by their cholesterol content and the presence of blood cells. *Biochem. Biophys. Res. Commun*., 89 (4) (1979), pp. 1287-1293.

[59]C. Kirby, J. Clarke, G. Gregoriadis. Effect of the cholesterol content of small unilamellar liposomes on their stability in vivo and in vitro. *Biochem. J.,* 186 (2) (1980), pp. 591-598.

[60]H. Chen, M.B. Müller, K.J. Gilmore, G.G. Wallace, D. Li. Mechanically strong, electrically conductive, and biocompatible graphene paper. *Adv. Mater*., 20 (18) (2008), pp. 3557-3561.

[61]Y.S. Al-Degs, M.I. El-Barghouthi, A.H. El-Sheikh, G.M. Walker. Effect of solution pH, ionic strength, and temperature on adsorption behavior of reactive dyes on activated carbon. *Dyes Pigments*, 77 (1) (2008), pp. 16-23.

[62]C. Shan, H. Yang, D. Han, Q. Zhang, A. Ivaska, L. Niu. Water-soluble graphene covalently functionalized by biocompatible poly-L-lysine. *Langmuir*, 25 (20) (2009), pp. 12030-12033.

[63]J.-Y. Chun, M.-J. Choi, S.-G. Min, J. Weiss. Formation and stability of multiple-layered liposomes by layer-by-layer electrostatic deposition of biopolymers. *Food Hydrocolloids*, 30 (1) (2013), pp. 249-257.

[64]H.J. Ploehn, C. Liu. Quantitative analysis of montmorillonite platelet size by atomic force microscopy. *Ind. Eng. Chem. Res*., 45 (21) (2006), pp. 7025-7034.

[65]D.L. Cooper, S. Harirforoosh Design and optimization of PLGA-based diclofenac loaded nanoparticles. *PLoS One*, 9 (1) (2014), p. e87326.

[66]Y.N. Konan, R. Cerny, J. Favet, M. Berton, R. Gurny, E. Allémann. Preparation and characterization of sterile sub-200 nm meso-tetra (4-hydroxylphenyl) porphyrin-loaded nanoparticles for photodynamic therapy. *Eur. J. Pharm. Biopharm*., 55 (1) (2003), pp. 115-124.

[67]V. Saxena, M. Sadoqi, J. Shao. Indocyanine green-loaded biodegradable nanoparticles: preparation, physicochemical characterization and in vitro release. *Int. J. Pharm*., 278 (2) (2004), pp. 293-301.

[68]H.-J. Yoon, T.G. Lim, J.-H. Kim, Y.M. Cho, Y.S. Kim, U.S. Chung, J.H. Kim, B.W. Choi, W.-G. Koh, W.-D. Jang. Fabrication of multifunctional layer-by-layer nanocapsules toward the design of theragnostic nanoplatform. *Biomacromolecules*, 15 (4) (2014), pp. 1382-1389.

[69]V. Mohanta, G. Madras, S. Patil. Layer-by-layer assembled thin film of albumin nanoparticles for delivery of doxorubicin. *J. Phys. Chem.* C, 116 (9) (2012), pp. 5333-5341.

[70]W. Liu, J. Liu, W. Liu, T. Li, C. Liu. Improved physical and in vitro digestion stability of a polyelectrolyte delivery system based on layer-by-layer self-assembly alginate–chitosan-coated nanoliposomes. *J. Agric Food Chem*., 61 (17) (2013), pp. 4133-4144.

[71]S. Ye, C. Wang, X. Liu, Z. Tong. Multilayer nanocapsules of polysaccharide chitosan and alginate through layer-by-layer assembly directly on PS nanoparticles for release. *J. Biomater. Sci. Polym. Ed*., 16 (7) (2005), pp. 909-923.

[72]W. Qi, W. Yuan, J. Yan, H. Wang. Growth and accelerated differentiation of mesenchymal stem cells on graphene oxide/poly-L-lysine composite films*. J. Mater. Chem*. B, 2 (33) (2014), pp. 5461-5467.

[73]Z. Liu, Z. Guo, H. Zhong, X. Qin, M. Wan, B. Yang. Graphene oxide based surface-enhanced Raman scattering probes for cancer cell imaging. *Phys. Chem. Chem. Phys*., 15 (8) (2013), pp. 2961-2966.

[74]R. Pignatello, I. Toth, G. Puglisi. Structural effects of lipophilic methotrexate conjugates on model phospholipid biomembranes. Thermochim. Acta, 380 (2) (2001), pp. 255-264.

[75]R.B. Campbell, S.V. Balasubramanian, R.M. Straubinger. Phospholipid-cationic lipid interactions: influences on membrane and vesicle properties. *Biochim. Biophys. Acta*, 1512 (1) (2001), pp. 27-39.

[76]S. Ohtake, C. Schebor, J.J. de Pablo. Effects of trehalose on the phase behavior of DPPC–cholesterol unilamellar vesicles. *Biochim. Biophys. Acta*, 1758 (1) (2006), pp. 65-73.

[77]V. Krikorian, M. Kurian, M.E. Galvin, A.P. Nowak, T.J. Deming, D.J. Pochan. Polypeptide-based nanocomposite: Structure and properties of poly (L-lysine)/Na+-montmorillonite. *J. Polym. Sci.* Part B, 40 (22) (2002), pp. 2579-2586.

[78]S. Park, J. An, J.R. Potts, A. Velamakanni, S. Murali, R.S. Ruoff. Hydrazine-reduction of graphite-and graphene oxide. *Carbon*, 49 (9) (2011), pp. 3019-3023.

[79]Y. Wang, J. Liu, L. Liu, D.D. Sun. High-quality reduced graphene oxide-nanocrystalline platinum hybrid materials prepared by simultaneous co-reduction of graphene oxide and chloroplatinic acid. *Nanoscale Res. Lett*., 6 (1) (2011), pp. 241-249.

[80]R.J. Lee, S. Wang, M.J. Turk, P.S. Low. The effects of pH and intraliposomal buffer strength on the rate of liposome content release and intracellular drug delivery. *Biosci. Rep*., 18 (2) (1998), pp. 69-78.

[81]X. Li, D. Cabral-Lilly, A. Janoff, W. Perkins. Complexation of internalized doxorubicin into fiber bundles affects its release rate from liposomes. *J. Liposome Res*., 10 (1) (2000), pp. 15-27.

[82]M. Karlina, O. Pozharitskaya, A. Shikov, V. Makarov, S. Mirza, I. Miroshnyk, R. Hiltunen. Drug synthesis methods and manufacturing technology. *Pharm. Chem. J*., 44 (9) (2010), pp. 34-36.

[83]A. Fritze, F. Hens, A. Kimpfler, R. Schubert, R. Peschka-Süss. Remote loading of doxorubicin into liposomes driven by a transmembrane phosphate gradient. *Biochim. Biophys. Acta*, 1758 (10) (2006), pp. 1633-1640.

[84]T. Ramasamy, T.H. Tran, H.J. Cho, J.H. Kim, Y.I. Kim, J.Y. Jeon, H.-G. Choi, C.S. Yong, J.O. Kim. Chitosan-based polyelectrolyte complexes as potential nanoparticulate carriers: physicochemical and biological characterization. *Pharm. Res*., 31 (5) (2014), pp. 1302-1314.

[85]M. Massignani, C. LoPresti, A. Blanazs, J. Madsen, S.P. Armes, A.L. Lewis, G. Battaglia. Controlling cellular uptake by surface chemistry, size, and surface topology at the nanoscale. *Small*, 5 (21) (2009), pp. 2424-2432.

[86]K.Y. Win, S.-S. Feng. Effects of particle size and surface coating on cellular uptake of polymeric nanoparticles for oral delivery of anticancer drugs. *Biomaterials*, 26 (15) (2005), pp. 2713-2722.

[87]C. He, Y. Hu, L. Yin, C. Tang, C. Yin. Effects of particle size and surface charge on cellular uptake and biodistribution of polymeric nanoparticles. *Biomaterials*, 31 (13) (2010), pp. 3657-3666.

[88]A. Albanese, P.S. Tang, W.C. Chan. The effect of nanoparticle size, shape, and surface chemistry on biological systems. *Ann. Rev. Biomed. Eng.,* 14 (2012), pp. 1-16.

[89]X. Zhang, W. Hu, J. Li, L. Tao, Y. Wei. A comparative study of cellular uptake and cytotoxicity of multi-walled carbon nanotubes, graphene oxide, and nanodiamond. *Toxicol. Res.,* 1 (1) (2012), pp. 62-68.

[90]B. Alberts, A. Johnson, J. Lewis, M. Ra, K. Roberts. *Molecular Biology of the Cell*. Garland Science Taylor & Francis Group, City (2002).

[91]O. Harush-Frenkel, N. Debotton, S. Benita, Y. Altschuler. Targeting of nanoparticles to the clathrin-mediated endocytic pathway. *Biochem*. *Biophys. Res. Commun*., 353 (1) (2007), pp. 26-32.

[92]B. Sun, S.-S. Feng. Trastuzumab-functionalized nanoparticles of biodegradable copolymers for targeted delivery of docetaxel. *Nanomedicine*, 4 (4) (2009), pp. 431-445.

[93]D.E. Reisner. *Bionanotechnology II: Global Prospects*. CRC Press, 2 (2011).

[94]B. Sun, B. Ranganathan, S.-S. Feng. Multifunctional poly (D, L-lactide-co-glycolide)/montmorillonite (PLGA/MMT) nanoparticles decorated by Trastuzumab for targeted chemotherapy of breast cancer. *Biomaterials*, 29 (4) (2008), pp. 475-486.

[95]M. Babic, D. Horák, M. Trchová, P. Jendelová, K. Glogarová, P. Lesný, V. Herynek, M. Hájek, E. Syková. Poly (L-lysine)-modified iron oxide nanoparticles for stem cell labeling. *Bioconj. Chem.,* 19 (3) (2008), pp. 740-750.

[96]V. Vaijayanthimala, Y.-K. Tzeng, H.-C. Chang, C.-L. Li. The biocompatibility of fluorescent nanodiamonds and their mechanism of cellular uptake. *Nanotechnology*, 20 (42) (2009), pp. 425103-425112.

[97]X.T. Zheng, X.Q. Ma, C.M. Li. Highly efficient nuclear delivery of anti-cancer drugs using a bio-functionalized reduced graphene oxide. *J. Colloid Interface Sci*., 467 (2016), pp. 35-42.